Immune Regulation of Intestinal Stem Cell Proliferation and Differentiation in *Drosophila*.

Minjeong Shin[1], Meghan Ferguson[1,2], Reegan J. Willms[1], Lena O. Jones[1], Kristina Petkau[1], and Edan Foley[1,2]*.

1: Department of Medical Microbiology and Immunology, Faculty of Medicine and Dentistry, University of Alberta, Edmonton, AB, Canada

2: Department of Cell Biology, Faculty of Medicine and Dentistry, University of Alberta, Edmonton, AB, Canada

*Corresponding Author: efoley@ualberta.ca

11 **HIGHLIGHTS**
12

13 - The TNFR-like Immune Deficiency (IMD) pathway is active in *Drosophila* intestinal progenitor cells.
14 - Inhibition of IMD in progenitors impairs progenitor cell proliferation.
15 - Blocking progenitor cell IMD negatively affects generation of mature epithelial cells.

16

ABSTRACT

Intestinal progenitor cells integrate signals from their niche, and from the gut lumen, to divide and differentiate at a rate that maintains an epithelial barrier to microbial invasion of the host interior. Despite the importance of evolutionarily conserved innate immune defenses to maintain stable host-microbiota relationships, we know little about specific contributions of stem cell immunity to gut homeostasis. We used the *Drosophila* model to determine the consequences of compromised intestinal stem cell immune activity for epithelial homeostasis. We showed that loss of stem cell immunity greatly impacted growth and renewal in the adult gut. In particular, we noticed that inhibition of stem cell immunity impeded key growth and differentiation events in the progenitor cell compartment leading to a gradual loss of stem cell numbers with age, and an impaired differentiation of mature enteroendocrine cells. Our results highlight the importance of immune signaling in the stem cell population for epithelial function in the adult gut.

INTRODUCTION

The intestinal epithelium is an important contact point between an animal and their environment. Collectively, intestinal epithelial cells regulate nutrient acquisition, microbiota tolerance, immune education, and pathogen elimination, and disruptions to epithelial homeostasis are linked to inflammatory diseases and cancers. As the epithelium consists of a heterogenous population of specialized cell types, it is essential that we understand the mechanisms by which individual lineages regulate intestinal cell proliferation, differentiation, and renewal.

Intestinal epithelial cell (IEC) lineages vary by animal, but data from *Drosophila*, zebrafish, mice, and humans indicate broad evolutionarily conservation of intestinal cell-type composition (Brugman, 2016; Buchon et al., 2013a; Lickwar et al., 2017; Miguel-Aliaga et al., 2018; Nguyen et al., 2015; Wallace et al., 2005). Typically, the epithelium is maintained by proliferative, multipotent Intestinal Stem Cells (ISCs) that self-renew, and generate all differentiated epithelial cell types. Most terminally differentiated cells are columnar enterocytes, a cell type specialized in capture and digestion of lumenal nutrients. Secretory cell-type complexity varies from animal to animal. In flies, the secretory lineage appears to consist solely of hormone-producing enteroendocrine cells. In contrast, fish and mammals have mucus-secreting goblet cells in addition to the enteroendocrine population, and mammals also have long-lived, antimicrobial peptide-producing Paneth cells that neighbor ISCs in basal crypts. ISCs integrate cues from their niche to divide and differentiate at a rate that replenishes dying epithelial cells, effectively maintaining gut function, and barrier integrity. Notch, Epidermal Growth Factor (EGF), Wnt and Bone Morphogenetic Protein (BMP) signal transduction pathways are particularly important regulators of ISC proliferation and differentiation in vertebrates and invertebrates (Spit et al., 2018). More recent studies uncovered roles for immune signaling in ISC survival, growth and differentiation. For example, vertebrate ISCs express MHC class II molecules, and presentation of self-peptides by ISCs appears to be a critical aspect of intestinal invasion and epithelial destruction in graft-versus host disease (Biton et al., 2018; Fu et al., 2019; Takashima et al., 2019). Likewise, ISCs are enriched for expression of the germline-encoded peptidoglycan receptor NOD2 (Nigro et al., 2014). NOD2 protects ISCs against reactive oxygen species toxicity (Levy et al., 2020),

54 and mutations in NOD2 are associated with Crohn's disease and intestinal tumorigenesis (Couturier-Maillard et
55 al., 2013). Despite established requirements for immune signaling pathways in the maintenance of intestinal
56 health, it is unclear if innate defenses act specifically in progenitors to regulate epithelial homeostasis. We
57 consider this an important knowledge gap given the central role of intestinal progenitors in building and
58 maintaining the entire epithelium.
59
60 *Drosophila melanogaster* are widely used to characterize intestinal epithelial immunity and homeostasis. The
61 adult fly intestine is a pseudostratified epithelium that is maintained by multipotent ISCs (Micchelli and Perrimon,
62 2006; Ohlstein and Spradling, 2006). The majority of *Drosophila* ISC divisions are asymmetric, producing a new
63 ISC, and a transient cell type that generates terminally differentiated epithelial cells. In most cases, ISC divisions
64 generate a post-mitotic enteroblast that differentiates as an enterocyte in response to Notch signals (Bardin et
65 al., 2010; Guo and Ohlstein, 2015; Ohlstein and Spradling, 2007). Collectively, ISCs and enteroblasts are classified
66 as the intestinal progenitor compartment in flies. Alternatively, in the absence of cues from Notch, ISCs transition
67 through a pre-enteroendocrine state to generate mature enteroendocrine cells that can be sub-classified into
68 functional groups based on intestinal localization, and hormone expression patterns (Biteau and Jasper, 2014; Guo
69 and Ohlstein, 2015; Zeng and Hou, 2015). In the fly gut, bacterial diaminopimelic acid-type peptidoglycan (PGN)
70 activates immune responses via the Immune Deficiency (IMD) pathway, a germline-encoded defense with
71 similarities to vertebrate Tumor Necrosis Factor Receptor signaling (Buchon et al., 2009b, 2013a; Myllymäki et al.,
72 2014). Detection of extracellular polymeric PGN by the PGRP-LC receptor, or intracellular monomeric PGN by the
73 related PGRP-LE receptor converges on a proximal signaling complex that includes the Imd protein, the adaptor
74 protein FADD, and the Caspase-8 homolog, Dredd. Dredd proteolytically removes thirty N-terminal amino acids
75 from Imd, initiating molecular events that activate c-Jun N-terminal Kinase, and the p100/105 NF-kB ortholog
76 Relish (Rel) (Leulier et al., 2000; Stoven et al., 2003; Stöven et al., 2000). Thus, Dredd-mediated processing of Imd
77 is essential for IMD pathway activation, and expression of a non-cleavable Imd variant (ImdD30A) blocks host
78 responses to PGN in cell culture and *in vivo* (Kim et al., 2014; Paquette et al., 2010). In the fly intestine, Rel and c-

79 Jun N-terminal Kinase initiate transcriptional responses that include regionalized expression of antimicrobial
80 peptides, regulators of metabolism, and genes associated with growth and differentiation (Broderick et al., 2014;
81 Buchon et al., 2009b, 2009a; Dutta et al., 2015; Hung et al., 2020). Earlier work uncovered significant differences
82 between the responses of mature epithelial cell-types to IMD activation. For example, infection-dependent
83 activation of IMD in enterocytes results in antimicrobial peptide expression and extrusion of damaged cells
84 (Buchon et al., 2009b; Dutta et al., 2015; Zhai et al., 2018). In contrast, activation of IMD in enteroendocrine cells
85 by commensal-derived lactate modifies lipid metabolism in neighboring enterocytes (Kamareddine et al., 2018).
86 Notably, genomic studies demonstrated expression of IMD pathway components in intestinal progenitor cells
87 (Dutta et al., 2015; Hung et al., 2020). However, the contributions of progenitor-specific IMD activity to intestinal
88 homeostasis are unexplored.
89
90 We took advantage of the genetic accessibility of flies to ask if progenitor-specific IMD activity affects
91 intestinal homeostasis in adult *Drosophila*. Specifically, we used genomic and physiological assays to determine
92 the consequences of blocking IMD in intestinal progenitors. We found that inhibition of progenitor cell IMD had
93 significant effects on ISC proliferation, progenitor compartment composition, and generation of mature
94 enteroendocrine cells. As germline-encoded immune responses are known modifiers of vertebrate intestinal
95 epithelial growth, we believe our findings are of general relevance to understanding how host immune responses
96 control stem cell function in the intestine.
97

98 **RESULTS**

99 **Inhibition of IMD Affects the Intestinal Progenitor Cell Transcriptome**

100 In a single-cell RNA sequencing profile of adult female *Drosophila* intestines, we identified 620 cells that
101 expressed canonical progenitor markers such as *esg*, *Dl*, and *N* (Figure S1). Within the progenitor population, we
102 observed enriched expression of key IMD pathway components, including the peptidoglycan sensor *pgrp-lc*, the
103 NF-kB transcription factor *relish*, and the IMD pathway target *pirk* (Figure 1A, B). Our data match earlier reports
104 of IMD pathway gene expression in progenitors (Dutta et al., 2015; Hung et al., 2020), and raise the possibility that
105 immune signals contribute to progenitor cell function in the fly gut.

106 To test if IMD is functionally active in progenitors, we used the *esgGAL4*, *GAL80^{ts}*, *UASGFP* (*esg^{ts}*) fly line to
107 express a dominant inhibitory IMD protein (ImdD30A) in *Drosophila* progenitors (*esg^{ts}/D30A*) for ten days.
108 Notably, blocking IMD in progenitors did not prevent infection-mediated expression of IMD-responsive
109 antimicrobial peptides in enterocytes, demonstrating that inhibition of progenitor cell IMD does not affect IMD
110 activity in differentiated progeny (Figure S2). We then asked if blocking IMD has direct effects on the progenitor
111 population. Intestines of *esg^{ts}/D30A* and control *esg^{ts}/+* flies had similar distributions of small, GFP-positive cells
112 (Figure 1C) that rarely expressed the enteroendocrine cell marker, *prospero* (Figure 1D), confirming that GFP
113 exclusively marked progenitors in both lines. To measure effects of IMD inhibition on progenitors, we performed
114 RNAseq analysis of gene expression in FACS-purified GFP-positive cells from *esg^{ts}/D30A* and *esg^{ts}/+* flies (Figure
115 1E). We found that inactivation of IMD disrupted expression of 154 genes in progenitors (Figure 1F, table S1),
116 including key IMD pathway regulators (*pgrp-sd*, *pgrpsc1a*), glutathione metabolism genes required for
117 detoxification of xenobiotic substances, and 24 genes known to respond to the commensal microbiome (Broderick
118 et al., 2014) (Figure 1F-H). Notably, the impacts of IMD inhibition extended beyond conventional antimicrobial
119 responses and included diminished expression of genes associated with stem cell growth, and adhesion to the
120 niche, such as the growth regulator *Xrp1*, the asymmetric cell division regulator *miranda* (*mira*), and the effector
121 of extracellular matrix adhesion *Vinculin* (*Vinc*, Figure 1F-H), suggesting potential growth-regulatory roles for IMD
122 in progenitors.

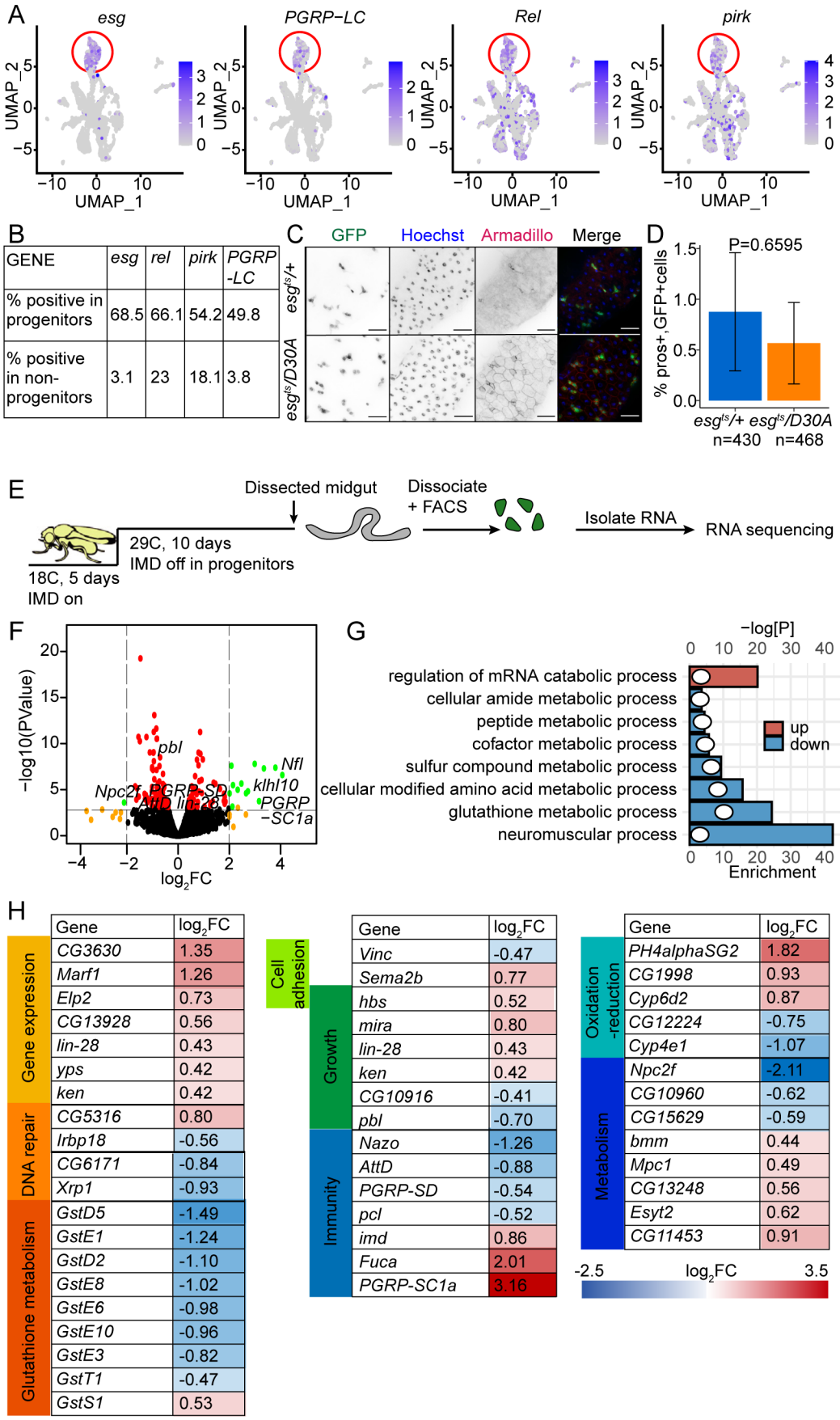

GENE	esg	rel	pirk	PGRP -LC
% positive in progenitors	68.5	66.1	54.2	49.8
% positive in non-progenitors	3.1	23	18.1	3.8

Gene	log_2FC
CG3630	1.35
Marf1	1.26
Elp2	0.73
CG13928	0.56
lin-28	0.43
yps	0.42
ken	0.42
CG5316	0.80
Irbp18	-0.56
CG6171	-0.84
Xrp1	-0.93
GstD5	-1.49
GstE1	-1.24
GstD2	-1.10
GstE8	-1.02
GstE6	-0.98
GstE10	-0.96
GstE3	-0.82
GstT1	-0.47
GstS1	0.53

Gene	log_2FC
Vinc	-0.47
Sema2b	0.77
hbs	0.52
mira	0.80
lin-28	0.43
ken	0.42
CG10916	-0.41
pbl	-0.70
Nazo	-1.26
AttD	-0.88
PGRP-SD	-0.54
pcl	-0.52
imd	0.86
Fuca	2.01
PGRP-SC1a	3.16

Gene	log_2FC
PH4alphaSG2	1.82
CG1998	0.93
Cyp6d2	0.87
CG12224	-0.75
Cyp4e1	-1.07
Npc2f	-2.11
CG10960	-0.62
CG15629	-0.59
bmm	0.44
Mpc1	0.49
CG13248	0.56
Esyt2	0.62
CG11453	0.91

123 Figure 1

124 **Figure 1. IMD Regulates the intestinal progenitor cell transcriptome.** (A) Uniform Manifold Approximation and
125 Projection (UMAP) plot of intestinal epithelial cells isolated from ten-day-old *esg*^{ts} flies showing expression of the
126 progenitor marker *esg*, and the IMD pathway components *PGRP-LC*, *Rel*, and *pirk*. Progenitors are circled in red.
127 (B) Quantification of the percentage of progenitors and non-progenitors that express the indicated genes. (C)
128 Visualization of GFP, DNA (Hoechst) and the beta-catenin ortholog in intestines of ten-day-old *esg*^{ts}*/+* and
129 *esg*^{ts}*/UAS-imdD30A (esg*^{ts}*/D30A*) flies. (D) Quantification of the percentage of GFP-positive cells that express the
130 enteroendocrine cell marker *prospero* in *esg*^{ts}*/+* (n=20) and *esg*^{ts}*/D30A* (n=22) flies. (E) Schematic representation
131 of an experimental strategy to quantify gene expression in progenitor cells purified from *esg*^{ts}*/+* and *esg*^{ts}*/D30A*
132 flies. Each experiment was performed in triplicate. (F) Volcano plot showing relative changes (x-axis) and
133 significance (y-axis) in gene expression of purified progenitors from *esg*^{ts}*/D30A* flies compared to age-matched
134 *esg*^{ts}*/+* controls. Genes are color coded to indicate significance and relative gene expression changes. (G) Gene
135 Ontology analysis of processes significantly affected by inhibition of IMD in progenitors. Column size indicates the
136 degree of enrichment for each term, and dots indicate the log-transformed significance of the respective
137 enrichment. (H) Representative sample of genes with affected expression upon inhibition of IMD in progenitors.
138

139 **Blocking IMD in Progenitors Inhibits ISC Division**

140 As IMD inhibition affected the progenitor cell transcriptome, we asked if IMD also affects progenitor cell
141 homeostasis. Specifically, we measured ISC mitoses by quantifying phospho-histone H3; the percentage of midgut
142 epithelial cells that expressed the progenitor marker *esg*; and the percentage of progenitors that expressed the
143 ISC marker *Delta* (*Dl*) in five and thirty-day-old *esg*^{ts}*/D30A* and *esg*^{ts}*/+* intestines. In young *esg*^{ts}*/+* intestines, we
144 observed few ISC divisions (Figure 2A), approximately 20% *esg*+ cells in the posterior midgut (Figure 2B), and 40%
145 Dl+ ISCs per progenitor (Figure 2C). Consistent with reports of age-related decline in gut function, we detected
146 significantly increased numbers of ISC divisions, *esg*+ cells, and Dl+ cells in aged *esg*^{ts}*/+* intestines relative to their
147 five-day-old counterparts (Figure 2A-C). In contrast, we did not detect age-dependent increases in mitoses,
148 progenitor number, or ISC numbers in thirty-day-old *esg*^{ts}*/D30A* intestines compared to their five-day-old

149 counterparts (Figure 2A-C). Instead, thirty-day-old *esg^{ts}/D30A* intestines were characterized by significantly fewer
150 mitoses, Dl+ ISCs, and progenitors than thirty-day-old *esg^{ts}/+* control flies. Importantly, these results are not an
151 artifact of *imdD30A* expression, as progenitor-specific, RNAi-mediated depletion of the IMD pathway adaptor
152 FADD also caused a significant decline in the amounts of Dl-positive stem cells among intestinal progenitors of
153 thirty-day-old flies (Figure 2D). Furthermore, we found that progenitor-specific inactivation of *relish* significantly
154 impaired generation of mitotic clones in the posterior midgut (Figure 2E), confirming that genetic inhibition of
155 IMD blocks intestinal epithelial proliferation. ISC-specific inactivation of IMD was sufficient to block proliferation
156 (Figure 2F), whereas EB-specific inhibition of IMD had no effect (Figure 2G), suggesting a cell-autonomous role for
157 IMD in controlling the rate of ISC division. Finally, we discovered that inhibition of the PGN sensors *PGRP-LC* or
158 *PGRP-LE* (Figure 2H-I) was sufficient to inhibit progenitor cell proliferation. Collectively, our data indicate that
159 inactivation of IMD in progenitors significantly impairs age-dependent accumulation of mitotically active
160 progenitors in the adult midgut. We consider these findings particularly interesting, as increased epithelial
161 immune responses are a hallmark of the aging intestine (Broderick et al., 2014; Buchon et al., 2009a; Guo et al.,
162 2014; Ren et al., 2007).
163

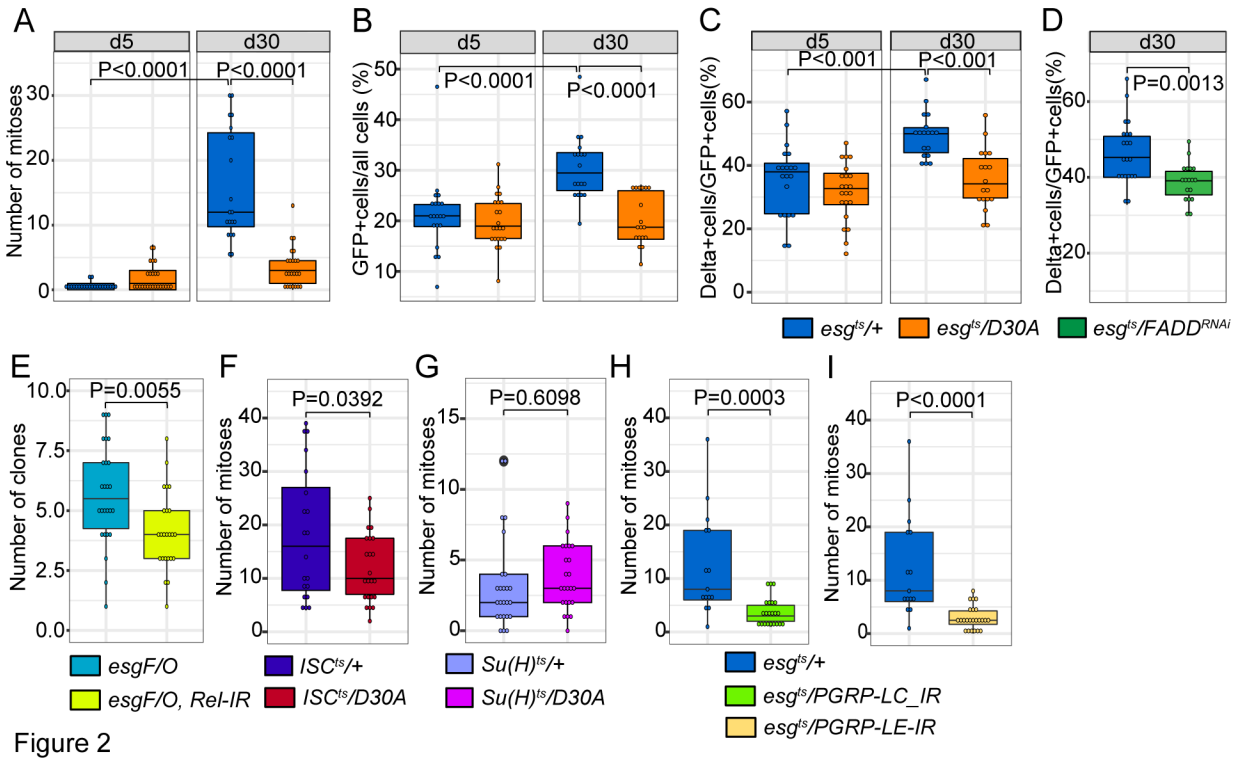

Figure 2

Figure 2: Progenitor cell IMD activity modifies stem cell proliferation. (A) Quantification of mitoses per gut in intestines from *esg^{ts}/+* and *esg^{ts}/D30A* flies of the indicated ages. (B) Percentage of intestinal epithelial cells that express the progenitor marker *esg* in *esg^{ts}/+* and *esg^{ts}/D30A* flies. (C) Percentage of progenitors that express the stem cell marker Delta in *esg^{ts}/+* and *esg^{ts}/D30A* flies. For A-C n=20 at d5, and 18 at d30 in *esg^{ts}/+* flies and n=22 at d5, and 18 at d30 in *esg^{ts}/D30A* flies. (D) Percentage of progenitors that express the stem cell marker Delta in *esg^{ts}/+* (n=21) and *esg^{ts}/FADD^{RNAi}* (n=18) flies. (E) Quantification of GFP-marked mitotic clones in the posterior midgut of *esg$^{F/O}$* (n=26) and *esg$^{F/O}$*, *rel-IR* (n=24) flies nine days after marking of mitotic clones. (F) Quantification of mitoses per gut in *ISC^{ts}/+* (n=21) and *ISC^{ts}/D30A* (n=24) 27 days flies. (G) Quantification of mitoses per gut in 27-day-old *Su(H)^{ts}*/+ (n=25) and *Su(H)^{ts}/D30A* (n=24) flies. (H-I) Quantification of mitoses per gut in 27-day-old *esg^{ts}/+* (n=15), *esg^{ts}/PGRP-LC-IR* (n=22) (H) and *esg^{ts}/PGRP-LE-IR* (I) flies. Statistical significance for A-C was calculated using an ANOVA followed by pairwise Tukey comparisons, and significance for D-I was calculated using a Student's t-test.

179 **Single Cell Transcriptional Profiles Uncover Impacts of Progenitor Cell IMD on the Intestinal Epithelium.**

180 Similar to vertebrates, the *Drosophila* intestine is a highly heterogenous tissue. Multipotent stem cells generate
181 distinct epithelial lineages that control nutrient acquisition, hormone production, and responses to intestinal
182 microbes in a regionally specialized fashion. Thus, although our data implicate IMD in progenitor cell division, we
183 do not yet understand the consequences of blocking IMD in progenitors for the entire intestine. To determine the
184 effects of progenitor-specific IMD inhibition on all epithelial cell types, we resolved the transcriptomes of ten-day-
185 old control *esg*^{ts}/+ and *esg*^{ts}*/D30A* intestines at the single cell level (Figure S3A-B). After excluding dead cells and
186 doublets, we prepared single-cell RNA sequencing profiles of 3675 cells from *esg*^{ts}/+ intestines, and 3654 cells
187 from *esg*^{ts}*/D30A* intestines. Using unsupervised graph-based clustering of data from *esg*^{ts}/+ intestines, we
188 identified all cell types previously described in the adult gut, including progenitors that expressed growth and
189 differentiation regulators; enteroendocrine cells that produced peptide hormones; and enterocytes dedicated to
190 digestion (Figure S3). A more detailed examination of single cell transcriptomes from *esg*^{ts}/+ intestines uncovered
191 clear signs of specialization among the individual cell types. Specifically, we discovered regionalized and cell-type-
192 specific expression patterns for regulators of metabolism (Figure S4), growth (Figure S5), differentiation (Figure
193 S6), peptidoglycan sensing and scavenging (Figure S7), and oxidative stress responses (Figure S8). Thus, our profile
194 of *esg*^{ts}/+ guts accurately recapitulated known features of spatial and functional specialization within the fly gut
195 (Dutta et al., 2015; Hung et al., 2020), providing a reliable control for analysis of intestines with impaired
196 progenitor cell IMD.

197 To determine if blocking IMD in progenitors affects the identity or function of mature epithelial cell types, we
198 used the integrated data analysis workflow in Seurat to identify cell type-specific differences in gene expression
199 patterns between *esg*^{ts}/+ and *esg*^{ts}*/D30A* intestines. Unsupervised clustering of the integrated data resolved
200 distinct clusters of progenitors, enterocytes, and enteroendocrine cells, as well as cardia, copper cells, an
201 enterocyte-like cluster, a cluster of immature enterocytes, and three lineages of unknown function (Figure 3B).
202 Comparisons between the two genotypes suggested mild effects of blocking IMD in progenitors on the generation
203 of mature intestinal epithelial cells. For example, we noted fewer EC-like cells, and considerably more cardia in

204 intestines from *esg*^{ts}*/D30A* than in *esg*^{ts}*/+* flies (Figure 3B). Furthermore, blocking IMD in progenitors had
205 significant effects on expression of genes associated with critical regulatory functions in the gut. For example,
206 intestines from *esg*^{ts}*/D30A* flies were characterized by shifts in RNA processing and translation in enterocytes,
207 diminished precursor metabolite generation in enteroendocrine cells, and increased expression of genes involved
208 in autophagy, cell polarity, and adhesion in progenitors (Figure 3C). Notably, blocking IMD in progenitors did not
209 affect expression of antimicrobial peptides, or peptidoglycan recognition proteins in differentiated enterocytes
210 (Table S2), further arguing that expression of *imdD30A* in progenitor cells does not inhibit immune activity in
211 progeny. Instead, we observed substantial effects of inhibiting IMD on expression of genes with essential roles in
212 progenitor cell division and polarity (Figure 3D), including the Notch signaling modifier *Npc2f*, the Notch pathway
213 target *E*(*spl*)*m3-HLH*, and *Snakeskin* (*Ssk*) a key regulator of intestinal stem cell activity (Figure 3E). Thus, and
214 consistent with data presented in Figures 1 and 2, our results indicate that inhibition of IMD in progenitors has
215 significant effects on progenitor cell homeostasis.

216 As we believe our gene expression data are likely useful of value to the community outside the scope of the
217 current study, we have deposited both sets on the Broad Institute Single Cell Portal (see Materials and Methods
218 for further details).

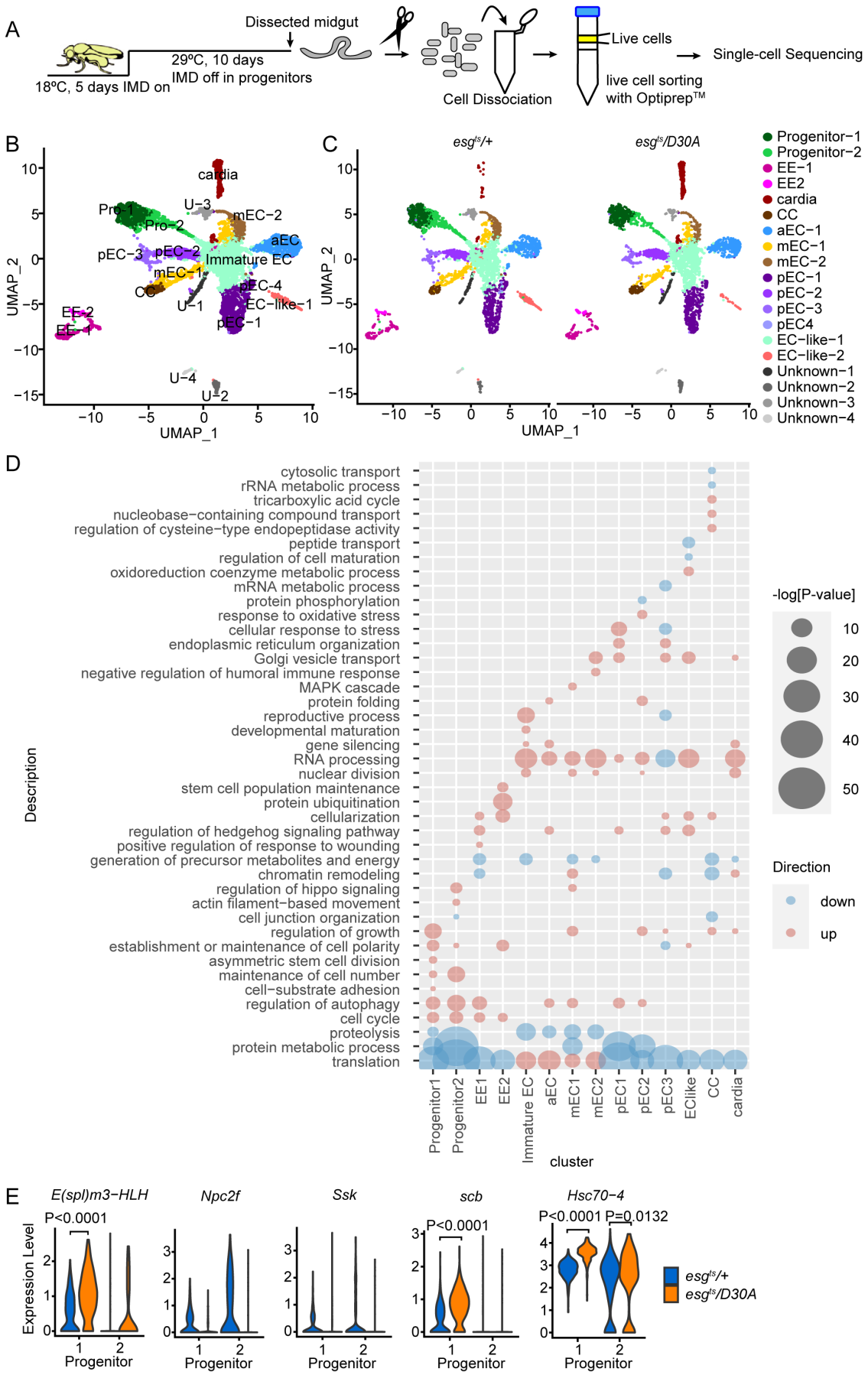
A
Dissected midgut
29ºC, 10 days
IMD off in progenitors
18ºC, 5 days IMD on
Cell Dissociation
Live cells
live cell sorting
with Optiprep™
Single-cell Sequencing
B
C
esg^ts/+
esg^ts/D30A
UMAP_1
UMAP_2
cardia
Pro-1
Pro-2
U-3
mEC-2
aEC
pEC-3
pEC-2
Immature EC
mEC-1
CC
pEC-4
EC-like-1
U-1
pEC-1
EE-2
EE-1
U-4
U-2
Progenitor-1
Progenitor-2
EE-1
EE2
cardia
CC
aEC-1
mEC-1
mEC-2
pEC-1
pEC-2
pEC-3
pEC4
EC-like-1
EC-like-2
Unknown-1
Unknown-2
Unknown-3
Unknown-4
D
Description
cytosolic transport
rRNA metabolic process
tricarboxylic acid cycle
nucleobase-containing compound transport
regulation of cysteine-type endopeptidase activity
peptide transport
regulation of cell maturation
oxidoreduction coenzyme metabolic process
mRNA metabolic process
protein phosphorylation
response to oxidative stress
cellular response to stress
endoplasmic reticulum organization
Golgi vesicle transport
negative regulation of humoral immune response
MAPK cascade
protein folding
reproductive process
developmental maturation
gene silencing
RNA processing
nuclear division
stem cell population maintenance
protein ubiquitination
cellularization
regulation of hedgehog signaling pathway
positive regulation of response to wounding
generation of precursor metabolites and energy
chromatin remodeling
regulation of hippo signaling
actin filament-based movement
cell junction organization
regulation of growth
establishment or maintenance of cell polarity
asymmetric stem cell division
maintenance of cell number
cell-substrate adhesion
regulation of autophagy
cell cycle
proteolysis
protein metabolic process
translation
Progenitor1
Progenitor2
EE1
EE2
Immature EC
aEC
mEC1
mEC2
pEC1
pEC2
pEC3
EClike
CC
cardia
cluster
-log[P-value]
10
20
30
40
50
Direction
down
up
E
E(spl)m3-HLH
Npc2f
Ssk
scb
Hsc70-4
P<0.0001
P<0.0001
P<0.0001
P=0.0132
Expression Level
Progenitor
esg^ts/+
esg^ts/D30A

Figure 3

220 **Figure 3. Inactivating IMD in progenitors affects transcriptional activity in all intestinal epithelial cell types.** (A)
221 Schematic representation of an experimental strategy for single-cell transcriptomic analysis of purified intestinal
222 epithelial cells from *esg*^{ts}*/+* and *esg*^{ts}*/D30A* flies. (B) UMAP plot visualizing cell-types in integrated data from *esg*^{ts}*/+*
223 and *esg*^{ts}*/D30A* flies based on the expression of marker genes. Cells are color coded by cell type. (C) The same
224 data from panel B, split into the labeled genotypes. EE = enteroendocrine cells. CC = copper cells. EC = enterocytes
225 subdivided according to anterior-posterior distribution along the intestine (a = anterior, m = middle, p = posterior).
226 (D) Gene Ontology term analysis of cell-type specific processes significantly affected by progenitor-restricted
227 inhibition of IMD. Bubble size indicates the log-transformed significance of the respective enrichments. Pink
228 bubbles indicate enhanced terms, blue bubbles indicate underrepresented terms. € Representative violin plots of
229 expression levels for the indicated genes in progenitors of *esg*^{ts}*/+* and *esg*^{ts}*/D30A* flies. P-values indicate
230 significantly different expression levels. For *Npc2f* and *Snakeskin* (*Ssk*), no expression was observed in progenitors
231 of *esg*^{ts}*/D30A* flies.
232
233 **Inhibition of IMD Affects Developmental Trajectories Within the Progenitor Compartment.**
234 We were intrigued by our observation that blocking IMD in progenitors significantly affected expression of genes
235 required for progenitor-niche interactions, and for progenitor differentiation. Therefore, we used Monocle to
236 prepare developmental trajectories for *esg*^{ts}*/+* and *esg*^{ts}*/D30A* intestines in pseudotime. Analysis of the respective
237 datasets successfully re-created developmental transitions from multipotent progenitors to differentiated
238 lineages in both lines (Figure 4A, D). To directly examine effects of IMD on progenitors, we created subsets of the
239 progenitor population for each genotype and analyzed gene expression in pseduotime for the respective subsets.
240 Examination of the progenitor population from both genotypes revealed gene expression patterns characteristic
241 of developmental transitions along a pseudotime trajectory (Figure 4B, E). For example, both progenitor
242 populations were characterized by expression of the ISC marker *Dl* in early stages of pseudotime (Figure 4C, F).
243 However, we found that IMD inhibition resulted in premature and prolonged pseudotime expression of the Notch
244 targets *E(spl)m3-HLH* (Figure 4G-H) and *E(spl)malpha-BFM* (Figure 4I-J), the EGF receptor inhibitor *sprouty* (*sty*,

245 Figure 4K-L), the EC fate regulator *klumpfuss* (*klu*, Figure 4M-N) and numerous markers of enterocyte maturation
246 (Figure S9), indicating effects of progenitor cell IMD activity on enterocyte differentiation. To test if blocking IMD
247 in progenitors has functional impacts on the transition from ISC to enteroblast, we monitored expression of
248 fluorescent markers in *esgGAL4*, *UAS-CFP*, *Su(H)-GFP ; GAL80*^{ts} flies that expressed ImdD30A. In these flies, ISCs
249 are visible as CFP-positive cells (pseudo-colored as yellow), and enteroblasts are visible as CFP and GFP double-
250 positive cells (pseudo-colored as magenta). Consistent with putative interactions between IMD and Notch
251 signaling, we found that blocking IMD significantly increased the percentage of progenitors that expressed the
252 enteroblast marker *Su*(*H*)-*GFP* (Figure 4O-P). Thus, in agreement with the loss of ISCs noted in *esg*^{ts}*/D30A*
253 intestines (Figure 2), our data argue that IMD activity influences progenitor cell composition in the fly intestinal
254 epithelium.
255

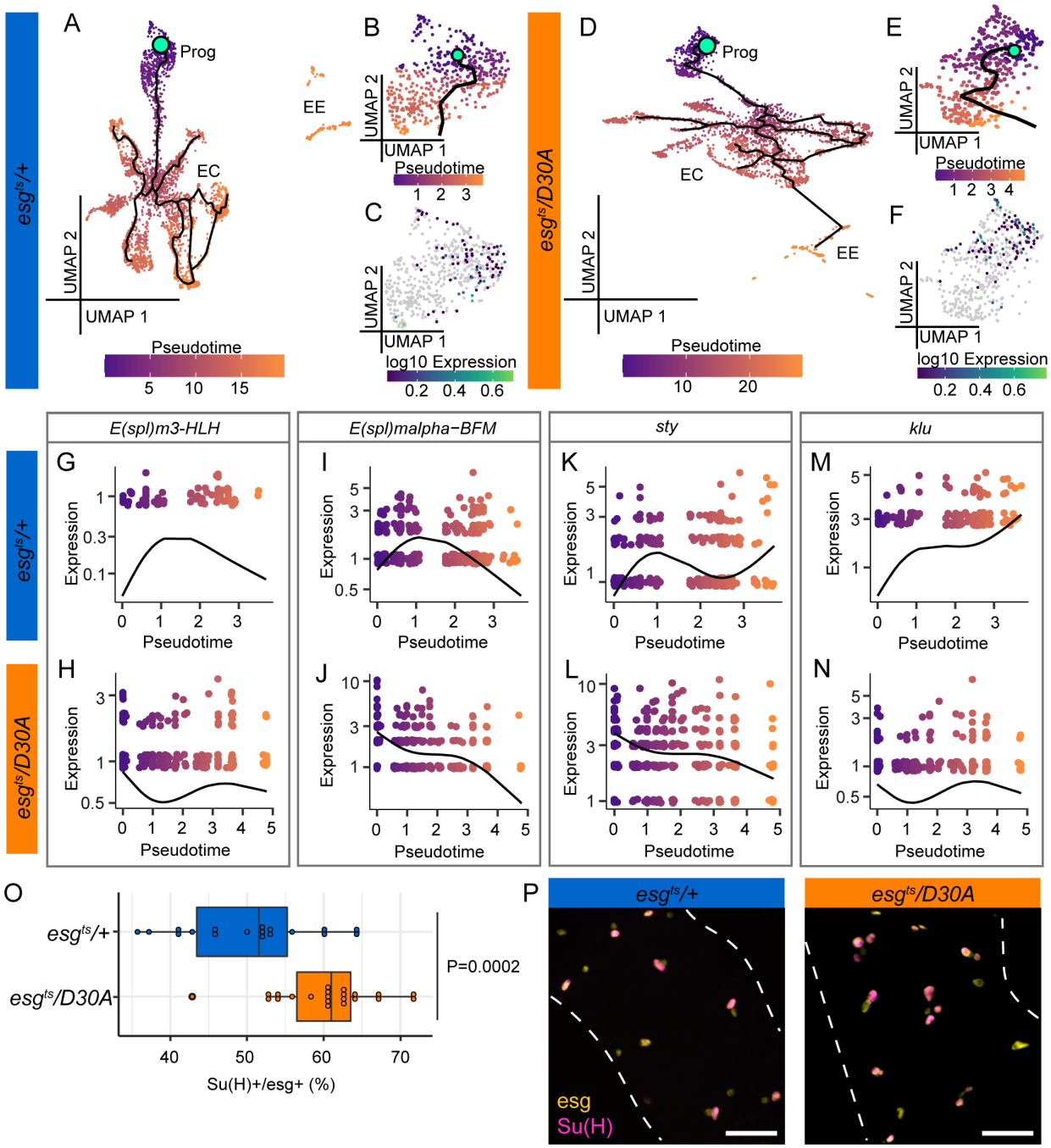

Figure 4. Inhibition of IMD affects developmental trajectories within the progenitor compartment. Single cell datasets from Seurat for each individual genotype were loaded into Monocle3 and pseudotime analysis was performed on midgut epithelial cells. (A) *esg^{ts}/+* midguts with wild-type progenitors and (D) *esg^{ts}/D30A* midguts with IMD-deficient progenitors. Mint green circles denote the root node and beginning of the intestinal trajectories. Dark purple marks cells at the beginning of pseudotime while orange marks cells late in pseudotime. Black lines show trajectories. Prog = Progenitors, EC = Enterocytes, EE = enteroendocrine cells. (B) and (E) show

263 pseudotime within progenitor subsets of (A) and (D) respectively. (C, F) *Delta (Dl*) expression patterns within
264 *esg^{ts}/+* progenitors (C) and *esg^{ts}/D30A* progenitors (F). Grey dots are cells with no detectable expression. (G-N)
265 Expression of Notch target genes *E(spl)m3-HLH, E(spl)malpha-BFM*, the EGF inhibitor *sprouty (sty*), and the EC fate
266 regulator *klumpfuss* (*klu*) over pseudotime within progenitor subsets of the indicated genotypes. (O) Percent of
267 *esg+* progenitors that are positive for the enteroblast marker *Su(H)+* in *esg^{ts}, UAS-CFP, Su(H)-GFP/+* (n=18) and
268 *esg^{ts}, UAS-CFP, Su(H)-GFP /D30A* (n=22) posterior midguts 14 days after transgene expression. Significance found
269 using Students t-test. (P) Representative images of intestines used to gather data for panel O.
270
271 **Inhibition of Progenitor Cell IMD Affects Generation of Mature Enteroendocrine Cells.**
272 IMD inhibition impaired ISC proliferation, diminished ISC numbers, and impacted cell-type composition within
273 the *esg*+ progenitor compartment, suggesting possible effects of progenitor cell IMD on development of mature
274 epithelial cells. To determine if inhibition of IMD in progenitors affects epithelial differentiation, we monitored
275 the prospero-positive enteroendocrine (EE) cell population in *esg^{ts}/+* and *esg^{ts}/D30A* intestines. We focused on EE
276 cells, as fly EE cells have been characterized to a single-cell resolution (Guo et al., 2019; Hung et al., 2020),
277 permitting detailed comparisons between *esg^{ts}/+* and *esg^{ts}/D30A* intestines. *Drosophila* EE cells can be divided
278 into subsets with distinct peptide hormone expression profiles that are stable during homeostasis or after recover
279 from infection (Beehler-Evans and Micchelli, 2015). Therefore, we tested if inhibition of IMD in progenitors
280 affected the representation of EE subsets in the intestine. Using unsupervised clustering of *prospero*-positive cells
281 from *esg^{ts}/+* and *esg^{ts}/D30A* intestines, we found that EE cells clustered into five subsets in both genotypes (Figure
282 5A, B). In both genotypes, each EE subset had a signature hormone expression pattern (Figure 5C, D). In some
283 cases, subset-restricted expression patterns were conserved between *esg^{ts}/D30A* and *esg^{ts}/+* EE cells. For
284 example, matching an earlier characterization of EE subsets (Beehler-Evans and Micchelli, 2015), we found that
285 cells from *esg^{ts}/+* subset zero, and from *esg^{ts}/D30A* subset two expressed *Tk* and *Dh31*. Likewise, *esg^{ts}/+* subset
286 three cells and *esg^{ts}/D30A* subset one cells were characterized by enhanced expression of *NPF*, and partial
287 expression of *Gbp5* and *CCAP*. In contrast, we did not detect a counterpart of *esg^{ts}/D30A* subset zero cells in *esg^{ts}/+*

288 controls, and we saw minimal conservation of *esg^{ts}/+* subset zero gene expression patterns in *esg^{ts}/D30A* EE cells,
289 suggesting functional differences between EE cells in *esg^{ts}/D30A* flies compared to *esg^{ts}/+* flies. When we classified
290 EE cells based on the number of peptides they expressed, we noted further differences between *esg^{ts}/+* and
291 *esg^{ts}/D30A* intestines. In particular, fewer EE cells expressed zero, or one peptide, in *esg^{ts}/D30A* guts than in *esg^{ts}/+*
292 guts, and a greater proportion expressed two or more peptides (Figure 5E). Likewise, for thirteen of fourteen
293 peptides examined, a greater percentage of *esg^{ts}/D30A* EE cells expressed the respective peptide than *esg^{ts}/+*
294 controls (Figure 5F), indicating enhanced peptide expression in *esg^{ts}/D30A* flies. To directly test the effects of
295 blocking IMD in progenitors on peptide expression levels, we performed an RNAseq analysis of dissected midguts
296 from *esg^{ts}/D30A* and *esg^{ts}/+* flies. With the exceptions of *ITP* and *Gpb5*, we found that blocking IMD in progenitors
297 resulted in increased expression of the remaining twelve peptides (Figure 5G), confirming a link between IMD
298 inhibition and peptide hormone expression. Finally, we quantified EE numbers in posterior midguts of *esg^{ts}/+* and
299 *esg^{ts}/D30A* flies that we raised at 29°C for ten days. We found that inhibition of IMD in progenitors decreased the
300 proportion of mature EE cells by roughly 20% relative to *esg^{ts}/+* controls (Figure 5H). Combined, our results
301 establish that inhibition of progenitor cell IMD disrupts peptide hormone expression patterns in mature EE cells,
302 decreases the amount of total EE cells, and increases the expression of most peptide hormones, confirming a link
303 between progenitor cell IMD activity and EE cell development.
304

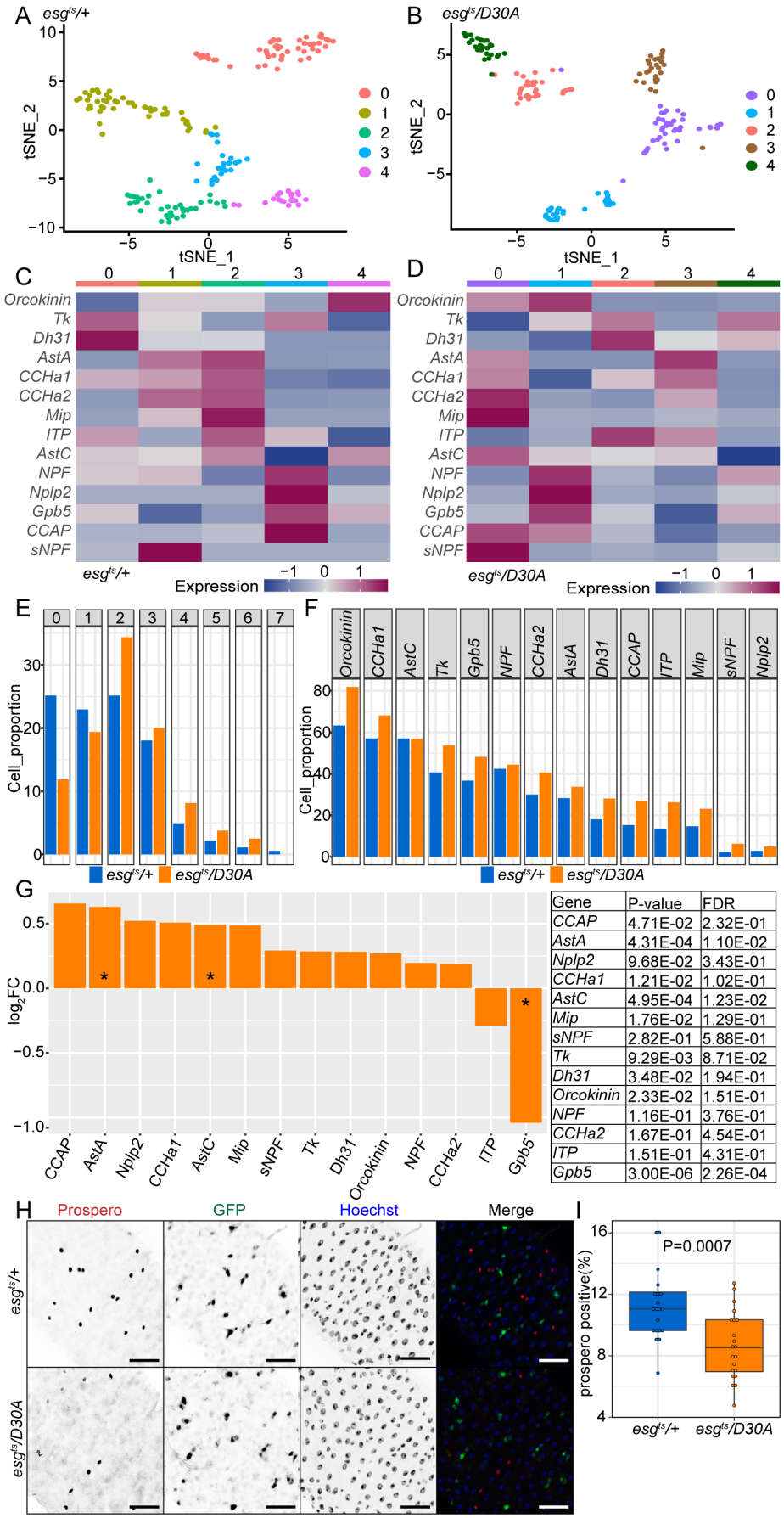

Gene	P-value	FDR
CCAP	4.71E-02	2.32E-01
AstA	4.31E-04	1.10E-02
Nplp2	9.68E-02	3.43E-01
CCHa1	1.21E-02	1.02E-01
AstC	4.95E-04	1.23E-02
Mip	1.76E-02	1.29E-01
sNPF	2.82E-01	5.88E-01
Tk	9.29E-03	8.71E-02
Dh31	3.48E-02	1.94E-01
Orcokinin	2.33E-02	1.51E-01
NPF	1.16E-01	3.76E-01
CCHa2	1.67E-01	4.54E-01
ITP	1.51E-01	4.31E-01
Gpb5	3.00E-06	2.26E-04

Figure 5

306 **Figure 5. (A-B)** tSNE plot visualizing subsets of *prospero*-positive enteroendocrine cells in *esg*^{ts}/*+* (A) and
307 *esg*^{ts}/*D30A* intestines (B) based on the expression of marker genes. Cells are color coded by cell subset. (C-D)
308 Heatmap showing relative expression of fourteen peptide hormones in each enteroendocrine cell subset in *esg*^{ts}/*+*
309 (C) and *esg*^{ts}/*D30A* (D) intestines. (E) Quantification of the percentage of enteroendocrine cells that express the
310 indicated numbers of peptide hormones. Genotypes are color coded as indicated. (F) Quantification of the
311 percentage of enteroendocrine cells that express the indicated peptide hormone. Genotypes are color coded as
312 indicated. (G) Quantification of the relative expression of each peptide hormone in isolated posterior midguts
313 from *esg*^{ts}/*D30A* flies relative to *esg*^{ts}/*+* flies based on bulk RNAseq analysis. (H) Visualization of Prospero, GFP and
314 DNA (Hoechst) in intestines of ten-day-old *esg*^{ts}/*+* and *esg*^{ts}/*D30A* flies. (I) Quantification of the percentage of
315 intestinal epithelial cells that express the enteroendocrine cell marker prospero in the intestines of ten-day-old
316 flies as indicated. Statistical significance was calculated using Students t-test. For *esg*^{ts}/*+* flies n=20, and for
317 *esg*^{ts}/*D30A* flies n=21.
318

319 **DISCUSSION**

320 Notch, BMP and WNT pathways regulate intestinal progenitor cell growth and differentiation in vertebrates
321 and invertebrates (Barker, 2014; Casali and Batlle, 2009; Miguel-Aliaga et al., 2018; Sancho et al., 2015; Vooijs et
322 al., 2011; Xu et al., 2011). In contrast, it is less clear what effects progenitor-specific activation of germline-
323 encoded immune response pathways has on epithelial homeostasis. Several studies indicated survival and growth-
324 regulatory effects of host immunity on intestinal progenitors. For example, the PGN pattern recognition receptor
325 NOD2 is enriched in ISCs of mice (Nigro et al., 2014), and NOD2 protects ISCs from irradiation-induced cytotoxicity
326 (Levy et al., 2020), while mutations in NOD2 are linked to Crohn's disease (Hugot et al., 2001; Ogura et al., 2001).
327 Likewise, TLR4 is expressed to higher levels in small and large intestinal crypts (Price et al., 2018), where its
328 activation promotes crypt apoptosis and inhibits proliferation (Naito et al., 2017; Neal et al., 2012). In contrast,
329 epithelium-wide activation of TLR4 promotes epithelial repair by activating EGF and JAK/STAT pathways in mice
330 challenged with dextran sulfate sodium (Fukata et al., 2006; Hsu et al., 2010). In combination, these studies
331 support roles for immune pathways in proliferative responses to cell-extrinsic challenges. However, we do not
332 know if progenitor-specific immune activity impacts homeostatic growth and differentiation. We consider this an
333 important question, as animal intestines contain dense microbial communities that promote growth and influence
334 cell fate choices in intestinal epithelia of animals as divergent as flies, fish, and mice (Ferguson and Foley, 2021).
335

336 We measured growth and differentiation in midguts of adult *Drosophila* that we engineered to lack IMD activity
337 in progenitors. The IMD pathway is highly similar to mammalian Tumor Necrosis Factor Receptor signaling, and
338 IMD exerts broad regulatory effects on intestinal transcription (Broderick et al., 2014). In flies, IMD has context-
339 dependent effects on ISC proliferation. IMD pathway mutants have elevated rates of mitoses that are driven by
340 the microbiome (Buchon et al., 2009b; Guo et al., 2014; Paredes et al., 2011), but IMD is not required for the
341 proliferative burst observed in flies challenged with *Ecc15* (Zhai et al., 2018). In contrast, infection with *Vibrio*
342 *cholerae* blocks ISC proliferation in an IMD-dependent manner (Fast et al., 2020; Wang et al., 2013), whereas
343 *Herpetomonas muscarum* induces IMD-dependent proliferation (Wang et al., 2019). In the absence of infectious

344 agents, persistent activation of IMD in progenitors increases ISC division frequency and skews differentiation
345 towards elevated numbers of enteroendocrine cells within the epithelium (Petkau et al., 2017). Similarly,
346 overexpression of PGRP-LC in enterocytes induces Rel-dependent proliferation (Zhai et al., 2018). There are
347 conflicting data on consequences of IMD inactivation in progenitors, with one study suggesting decreased
348 proliferation (Wang et al., 2019), and a separate study indicating increased proliferation (Wang et al., 2013). We
349 found that progenitor-specific inactivation of IMD diminished ISC proliferation, impaired age-dependent
350 accumulation of *esg*-positive and Dl-positive progenitors, elevated the number of *Su*(*H*)-positive enteroblasts, and
351 resulted in differentiation defects that included fewer enteroendocrine cells, and shifts in gene expression
352 patterns associated with enterocyte subtypes. Thus, our work suggests that progenitor-specific immune activity
353 contributes to epithelial homeostasis in flies and raises several questions about effects of progenitor cell IMD on
354 the adult gut.
355
356 Which progenitor cell requires IMD to regulate epithelial differentiation? In flies, the progenitor compartment
357 consists of undifferentiated ISCs, and post-mitotic enteroblasts that are committed to the enterocyte cell fate.
358 Adult progenitors express IMD pathway components, and genomic studies, including data presented here,
359 showed that ISCs and enteroblasts have highly similar gene expression profiles (Dutta et al., 2015; Hung et al.,
360 2020), suggesting that both cell types are likely equally competent at IMD activation. ISCs are basally situated
361 within the pseudostratified midgut epithelium, and are not expected to make frequent, direct contacts with the
362 intestinal lumen. Enteroblasts are the apical daughters of ISC divisions that occur at oblique angles to the
363 basement membrane. Thus, it seems more plausible that enteroblasts directly contact the lumen where they can
364 detect PGN. However, it is important to note that gut-derived PGN is not strictly contained to the intestinal lumen
365 in flies, or vertebrates. PGN crosses the intestinal epithelial barrier, even in the absence of detectable breaches,
366 and several mechanisms are in place to prevent accumulation of PGN in the fly hemolymph (Capo et al., 2017;
367 Gendrin et al., 2009; Paredes et al., 2011; Troha et al., 2019; Zaidman-Rémy et al., 2006). Thus, we cannot exclude
368 the possibility that passive, or active, transport mechanisms allow diffusion of PGN across the gut barrier to ISCs,

369 which in turn activate IMD and modulate differentiation responses in the hosts. In this regard, we consider it
370 interesting that several vertebrate pattern recognition receptors have cell-type specific apicobasal distribution
371 patterns. For instance, TLR4 is enriched apically in villi, and baso-laterally in crypts of the human colon (Fusunyan
372 et al., 2001). Furthermore, apical stimulation of TLR9 promotes JNK activation, whereas basolateral stimulation of
373 TLR9 leads to NF-kB activation, and IL-8 production (Lee et al., 2006). In future assays, it will be interesting to
374 determine if basolateral detection of PGN influences fate choices within the progenitor compartment.
375
376 Is progenitor-specific IMD necessary to generate growth-regulatory enterocytes? Inhibition of progenitor cell
377 IMD did not block IMD-dependent immune responses in enterocytes, confirming that the phenotypes reported
378 here are not a consequence of ImdD30A perdurance in differentiated epithelia. However, we also found that
379 inhibition of IMD in progenitors had consequences for epithelial differentiation, including effects on gene
380 expression patterns within mature enterocytes. As enterocytes produce paracrine regulators of progenitor
381 proliferation and differentiation, we cannot exclude the possibility that blocking IMD in progenitors disrupts
382 enteroblast differentiation in a manner that modifies the ability of enterocytes to transduce growth and
383 differentiation cues to progenitor cells. This may be particularly important in the context of severe epithelial
384 damage, where secreted factors from dying enterocytes accelerate ISC proliferation to maintain the epithelial
385 barrier and regenerate a mature gut. In this scenario, IMD activity in progenitors is important to establish
386 homeostatic intercellular communications between enterocytes and the progenitor compartment, and loss of
387 progenitor cell IMD interrupts a developmental loop between progenitors and enterocytes. Consistent with
388 requirements for IMD in the control of epithelial differentiation, we noticed that blocking IMD in progenitors
389 significantly affected the generation of mature enteroendocrine cells. Specifically, inhibition of progenitor cell IMD
390 led to a decline in enteroendocrine numbers, but a general increase in the expression of peptide hormones,
391 possibly as a compensatory mechanism. Notably, flies raised in an axenic environment have fewer enteroblasts
392 and more enteroendocrine cells (Broderick et al., 2014), indicating non-overlapping contributions of progenitor
393 cell immunity and gut microbes to developmental trajectories of ISCs.

394

395 Does IMD have regional effects on intestinal progenitor functions? Intestines are functionally specialized along
396 the rostro-caudal axis, with distinct partitions governing various aspects of food digestion and absorption. IMD
397 also displays clear signs of regional specialization. The foregut is characterized by enriched expression of PGRP-
398 LC, and Rel regulates expression of chitin-binding proteins that contribute to peritrophic matrix construction
399 (Buchon et al., 2009b; Neyen et al., 2012). In the midgut, PGN detection appears to rely primarily on PGRP-LE,
400 particularly in the posterior midgut (Bosco-Drayon et al., 2012; Neyen et al., 2012). Activation of IMD in the
401 anterior midgut results in expression of antimicrobial peptides that protect the fly from ingested microbes
402 (Buchon et al., 2013b). In contrast, IMD activation leads to delamination of damaged cells in the midgut of flies
403 infected with pathogenic bacteria, most notably in the R4 region of the posterior midgut (Zhai et al., 2018). In the
404 posterior midgut, the transcription factor caudal prevents IMD-dependent antimicrobial peptide expression (Ryu
405 et al., 2008). Instead, IMD induces expression of molecules that dampen immune signaling, including the PGRP-
406 LC inhibitor *pirk*, and amidases that scavenge PGN (Bosco-Drayon et al., 2012). As a result, posterior midgut IMD
407 activity establishes a tolerogenic environment for commensal bacteria. Notably, loss of IMD pathway inhibitors,
408 or expression of PGRP-LC in enterocytes increases proliferation in the posterior midgut (Paredes et al., 2011; Zhai
409 et al., 2018), raising the possibility that suppression of posterior midgut IMD activity is required to prevent excess
410 proliferation in the absence of infection. With a large collection of genetic reagents, and accessible genomic
411 methods, the fly is an excellent system to systematically characterize regional effects of immune responses on
412 progenitor cell function. Given the evolutionary conservation of immune responses, we believe the findings
413 reported in this study to be of relevance for understanding fundamental principles of immune-regulated intestinal
414 homeostasis.

415

416

417 **MATERIALS AND METHODS**

418

419 **Fly Husbandry**

420 Flies were raised on corn meal medium (Nutri-Fly Bloomington formulation,
421 https://bdsc.indiana.edu/information/recipes/bloomfood.html; Genesse Scientific) at 18°C or 25°C. All
422 experimental flies were adult virgin females kept under a 12h:12h light:dark cycle and maintained at 18°C during
423 collection then shifted to 29°C to express downstream genes as indicated. We used w^{1118} as a wildtype strain
424 and backcrossed *UAS-imdD30A* transgenic lines into the w^{1118} background for eight generations prior to use and
425 used standard husbandry methods to ensure that esg^{ts} (*esg-GAL4*, $tub\text{-}GAL80^{ts}$, *UAS-GFP*) flies had the same first
426 and third chromosomes as our w^{1118} line. Fly lines used in this study were: *w ;* $esg\text{-}GAL4,tubGAL80^{ts},UAS\text{-}GFP$
427 (referred to as esg^{ts}), $UAS\text{-}FADD^{RNAi}$(VDRC ID# 7926), w^{1118} (VDRC ID# 60000), *w;esg-GAL4,UAS-CFP, Su(H)-*
428 $GFP;tubGal80^{ts}$ (esg^{ts}*,UAS-CFP,Su(H)-GFP*), *GS 5961* (Mathur et al., 2010), *dpt-GFP*, *esg-GAL4, tubGAL80ts, UAS-*
429 *GFP;UAS-flp, Act>CD2>GAL4* (referred to as $esg^{F/O}$), *Esg[ts], Su(H) Gal80* (referred to as ISC^{ts}), $Su(H)GBE\text{-}Gal4^{ts}$
430 (referred to as $Su(H)^{ts}$), *PGRP-LE RNAi* (VDRC ID# 108199), *PGRP-LC RNAi* (VDRC ID# 101636), *Rel-RNAi* (VDRC ID#
431 49413), *40D-UAS* (control for VDRC KK lines, VDRC ID# 60101) . To induce GFP-marked mitotic clones using the
432 $esg^{F/O}$ system, flies of the indicated genotype were raised at 18°C for three days after eclosion, shifted to 29°C for
433 16h, then raised at 25°C for an additional nine days.

434

435 ***Ecc15* Oral Infection**

436 For oral infection with *Ecc15*, we incubated an overnight culture of *Ecc15* in LB (Difco™ Luria Broth Base, Miller,
437 241420) supplemented with NaCl (4.75g Fisher Scientific, BP358-212 per 500mL of LB Broth base) at 29°C with
438 shaking. Flies were starved (10 flies per vial) for 2 h before infection. *Ecc15* was pelleted at 1250g for 10 minutes
439 at 4°C and supernatant decanted. The harvested bacterial pellet was re-suspended in residual LB and an equivalent
440 volume of 5% sucrose in PBS. Flies were transferred into vials that contained a filter paper (Whatman™, Grade 3,
441 23mm, 1003-323) soaked with 150ml of the *Ecc15* culture on top of standard corn meal medium. Flies were

442 infected for 16h at 29°C with 12h:12h light:dark cycle. To activate the GeneSwitch (GS) system we added 100µl
443 RU486 (Mifepristone, M8046, Sigma) dissolved in 80% EtOH (5mg/ml) to the surface of standard fool and dried
444 overnight prior to addition of flies. For controls, we added 100µl of 80% EtOH to the surface of standard fool and
445 dried overnight prior to addition of flies. Flies were raised on treated food for 48h prior to infection.
446
447 **Immunofluorescence**
448 The number of PH-3 or Delta positive cells were analyzed with two-way ANOVA or unpaired Student's t-tests. We
449 used previously described immunofluorescence protocols to visualize posterior midguts (56). In brief, we used
450 anti-phospho-histone H3 (PH3, 1:1000, Millipore (Upstate), 06-570) immunofluorescence to quantify mitoses in
451 the midguts, and anti-Delta (1:100; Developmental Studies Hybridoma Bank (DSHB) C594.9B)
452 immunofluorescence to quantify stem cells in the R4/R5 region of the posterior midguts of virgin female flies that
453 we raised at 29°C. We also used anti-prospero (1:100, DSHB), anti-armadillo (1:100, DSHB) as primary antibodies
454 and Hoechst 33258 (1:500; Molecular Probes) for DNA staining. Secondary antibodies used: goat anti-mouse Alexa
455 Fluor 568 (1:500; Invitrogen), goat anti-rabbit 488 (1:500; Invitrogen). Tissue was mounted in Fluoromount (Sigma-
456 Aldrich F4680) and posterior midguts were visualized with a spinning disk confocal microscope (Quorum WaveFX;
457 Quorum Technologies Inc.). Images were collected as Z-slices and processed with Fiji software to generate a Z-
458 stacked image.
459
460 **Isolation of progenitor cell and RNA extraction**
461 Progenitor cells were isolated by fluorescence activated cell sorting (FACS) as previously described by Dutta et al.
462 (2013). Flies were raised at 29°C for 10 days. 100 fly guts per sample were dissected (malphighian tubules, foreguts,
463 hindguts and crops removed) and placed into ice-cold 1XPBS/DEPC-treated water. Guts were dissociated with
464 1mg/ml of elastase at 27°C with periodic pipetting for 1h. GFP-positive progenitor cells were collected based on
465 GFP fluorescence and size with a BD FACSAriaIII sorter. Cells were pelleted at 1200g for 5 minutes at 4°C and then
466 resuspended in 500µl Trizol. Samples were stored at -80°C until all three biological replicates were collected. RNA

467 was isolated via a standard Trizol-chloroform extraction and the RNA was sent on dry ice to the Lunenfeld-
468 Tanenbaum Research Institute (Toronto, Canada) for library construction and sequencing. The sample quality was
469 evaluated using Agilent Bioanalyzer 2100. TaKaRa SMART-Seq v4 Ultra Low Input RNA Kit for Sequencing was used
470 to prepare full length cDNA. The quality and quantity of the purified cDNA was measure with Bioanalyzer and
471 Qubit 2.0. Libraries were sequenced on the Illumina HiSeq3000 platform.
472
473 **Preparation of Single Cell Suspension for single cell RNAseq**
474 Single-cell suspension preparation method were followed (Hung et al., 2018) with a few modifications. Flies were
475 raised for 10 days at 29°C. Five guts were dissected at one time and moved to 1% BSA in PBS/DEPC-treated water.
476 Once twenty-seven guts were dissected, we transferred the guts to 200ml 1XPBS/DEPC-treated water on the back
477 side of a glass dissection plate (PYREX, 7220-85) and chopped with scissors. After mechanically fragmenting the
478 tissue, it was transferred to a 1.5 ml tube containing 100ml 1XPBS/DEPC-treated water then enzymatically
479 digested with elastase (final concentration 1mg/ml) at 27°C for 40 min with gentle pipetting every 10 min. The
480 single cell suspension was pelleted at 300g for 15 min at 4°C and cell pellet resuspended in 200ml 0.04%BSA in
481 1XPBS/DEPC-treated water. The cell suspension was filtered through a 70μm filter (300g for 1 min at 4°C).
482 Live cells were collected using OptiPrepTM Density Gradient Medium (SIGMA, D1556-250ML) using the
483 OptiPrepTM Application Sheet C13 protocol. Briefly, a 40% (w/v) iodixanol working solution was prepared with 2
484 volumes of OptiPrepTM and 1 volume of 0.04 %BSA in 1XPBS/DEPC-treated water. This working solution was used
485 to prepare a 22% (w/v) iodixanol solution in the same buffer. One volume of working solution was carefully mixed
486 with 0.45 volume of cell suspension by gently inversion. The cell suspension/working solution mixture was
487 transferred to a 15ml conical tube then topped up to 6 ml with working solution. The working solution/cell
488 suspension was overlaid with 3 ml of the 22% (w/v) iodixanol and the 22% iodixanol layer was overlaid with 0.5
489 ml of 0.04 %BSA in 1XPBS/DEPC. Viable cells were separated by density gradient created by centrifuging at 800 g
490 for 20 min at 20°C. Viable cells were harvested from the top interface (~500ul) and then diluted in 2 volumes (1ml)
491 of 0.04 %BSA in 1XPBS/DEPC-treated water. The iodixanol was removed by pelleting live cell suspension at 300 g

492 for 10 min at 4°C. Supernatant was decanted and cells were resuspended in the leftover 0.04 %BSA in 1XPBS/DEPC-
493 treated water. Viability and concentration were measured by 0.4% trypan blue (Gibco, 15250-061) and
494 hemocytometer. Libraries were generated with a 10X Genomics Single-cell Transcriptome Library kit.
495
496 **Bioinformatics**
497 For purified progenitor RNAseq studies, we obtained approximately 6 million reads per biological replicate. We
498 used FASTQC to evaluate the quality of raw, paired- end reads, and trimmed adaptors and reads of less than 36
499 base pairs in length from the raw reads using Trimmomatic version 0.36. We used HISAT2 version 2.1.0 to align
500 reads to the *Drosophila* transcriptome- bdgp6, and converted the resulting BAM files to SAM flies using Samtools
501 version 1.8. We counted converted files using Rsubread version 1.24.2 and loaded them into EdgeR. In EdgeR, we
502 filtered genes with counts less than 1 count per million and normalized libraries for size. Normalized libraries were
503 used to call genes that were differentially expressed among treatments. Genes with P-value < 0.05 and FDR < 0.05
504 were defined as differentially expressed. Principle component analysis was performed on normalized libraries
505 using Factoextra version 1.0.5, and Gene Ontology enRIchment anaLysis and visuaLizAtion tool (GORILLA) was
506 used to determine Gene Ontology (GO) term enrichment. Specifically, differentially expressed genes were
507 compared in a two-list unraked comparison to all genes output from edgeR as a background set, and redundant
508 GO terms were removed.
509 For single cell analysis, Cell Ranger v3.0 was used to align sequencing reads to the *Drosophila* reference
510 transcriptome (FlyBase, r6.30) and generate feature-barcode matrices. These matrices were analyzed using the
511 Seurat R package (version 3.2.3). Cells possessing <500 UMIs or >2500 UMIs were removed to reduce the number
512 of low- quality cells and doublets. Seurat was then used to normalize expression values and perform integrated
513 data cell clustering at a resolution of 0.5 with 15 principal components. Clusters were identified based on known
514 markers and previous single-cell analysis of the *Drosophila* intestine (https://www.flyrnai.org/scRNA/). For GO
515 term analysis of single cell data, Seurat was used to integrate $esg^{ts}/+$ and $esg^{ts}/D30A$ datasets and generate lists
516 of differentially expressed genes for each cluster. Both up- and down-regulated gene lists (p-value cut-off <0.05)

517 were analyzed in GOrilla to determine GO term enrichment. Differentially expressed genes were compared in a
518 two-list unranked comparison to all genes identified in the single- cell dataset. GO terms were then analyzed in
519 REVIGO (REduce and VIsualize Gene Ontology) to remove redundant GO terms. Top enriched GO terms are shown
520 for each cluster, as well as those same GO terms found in other clusters. EE subset analysis was followed at Guo
521 et al. (2019).
522 For Pseudotime analysis we used Monocle3 (version 0.2.0). Specifically, we converted the existing Seurat data
523 from each genotype separately into a Monocle cell data set of midgut epithelial cells and performed trajectory
524 analysis. We manually assigned the root node of the trajectory to the node at the tip of the Progenitor cluster for
525 each genotype. We then subset the trajectory branch that explains pseudotime within the Progenitor population
526 to perform all subsequent gene level analysis. Here, we manually assessed expression of genes along pseudotime
527 with known functions in ISC identity, division, and differentiation including genes that were differentially
528 expressed based off our Seurat analysis.
529
530 **Data availability**
531 Gene expression data have been submitted to the NCBI GEO database (GEO: SuperSeries GSE141897 (GSE171001
532 and GSE141896)). Single cell gene expression data for *esg*^{ts}*/+* flies
533 (https://singlecell.broadinstitute.org/single_cell/study/SCP1696/single-cell-expression-data-for-d-melanogaster-
534 wild-type-intestines) and for *esg*^{ts}*/D30A* flies
535 (https://singlecell.broadinstitute.org/single_cell/study/SCP1699/single-cell-expression-data-for-d-melanogaster-
536 intestines-with-immune-deficient-progenitor-cells#study-summary) are available for visualization on the Broad
537 Institute Single Cell Portal.
538

539 **ACKNOWLEDGEMENTS**

540 *Drosophila* lines were kindly provided by Dr. Shelagh Campbell, Dr. Lucy O'Brien, Dr. Bruce Edgar, Dr. Heinrich
541 Jasper and Dr. Bruno Lemaitre. We acknowledge microscopy support from Dr. Steven Ogg and Gregory Plummer
542 at the Faculty of Medicine and Dentistry Imaging core; flow cytometry support from Dr. Aja Rieger at the Faculty
543 of Medicine and Dentistry Flow Cytometry Core; and support with single-cell library preparation from Dr. Joaquin
544 Lopez-Orozco. We are grateful to Dr. David Fast for assistance with analysis of the RNAseq data. The authors wish
545 to thank Kin Chan at the Network Biology Collaborative Centre for the RNA-Seq service. Network Biology
546 Collaborative Centre is a facility supported by Canada Foundation for Innovation, the Ontarian Government, and
547 Genome Canada and Ontario Genomics (OGI-139). This work was supported by a grant from the Canadian Institute
548 of Health Research (Grant # PJT 159604). Minjeong Shin was supported by Basic Science Research Program
549 through the National Research Foundation of Korea (NRF) funded by the Ministry of Education
550 (2020R1A6A3A0303955511). Meghan Ferguson has funding through Alberta Innovates Graduate Student
551 Scholarships and an NSERC PGS-D.

552

553

554 **SUPPLEMENTARY DATA**

555

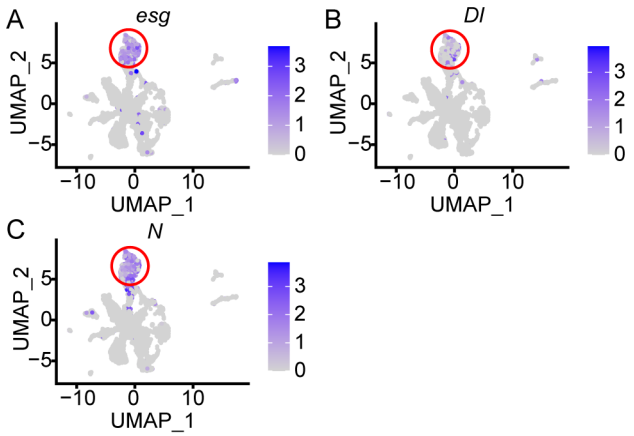

556 Figure S1

557

558 **Figure S1**: Feature plots showing expression of *Drosophila* progenitor cell markers *escargot* (*esg*), *Delta (Dl*), and

559 *Notch* (*N*) in an unsupervised UMAP prepared with single-cell expression data from adult esg^{ts}/+ female *Drosophila*

560 midguts. Progenitor cells are indicated with a red circle.

561

562

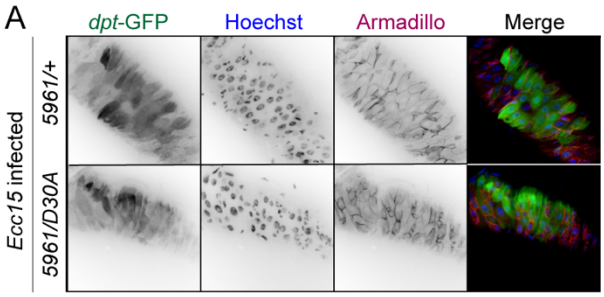

B

Genotype	Control	D30A
Sample size	9	10
% GFP +ive	100	100

Control: *GS 5961/+;dpt-GFP*
D30A: *GS 5961/D30A;dpt-GFP*

563 Supplementary Figure 2

564

565 **Figure S2 A:** Visualization of the IMD pathway reporter *diptericin:GFP* (*dpt*-GFP), DNA (Hoechst), and the beta-
566 catenin ortholog Armadillo in intestines of adult female *Drosophila* infected overnight with pathogenic *Ecc15*. The
567 *esg*^{ts} line used in the rest of the study marks progenitor cells with GFP, preventing us from unambiguously
568 identifying cells that expressed GFP under control of the *dpt* promoter in an *esg*^{ts} background. Therefore, we used
569 the *GS5961* gene switch fly line for RU486-dependent induction of the GAL4 transcription factor in intestinal
570 progenitor cells in this experiment. In the upper row, we visualized *dpt*-GFP expression in *GS5961/+* (*5961/+*) flies,
571 and in the lower row, we visualized *dpt*-GFP expression in *GS5961/UAS-imdD30A* (*5961/D30A*) flies. Both lines
572 were treated with RU486 for 48h prior to infection. **B:** Quantification of fly guts of the indicated genotypes that
573 expressed *dpt*-GFP in enterocytes after infection with *Ecc15.* Expression of imdD30A in progenitors (*D30A*) did not
574 prevent infection-mediated activation of IMD responses in mature enterocytes.

575

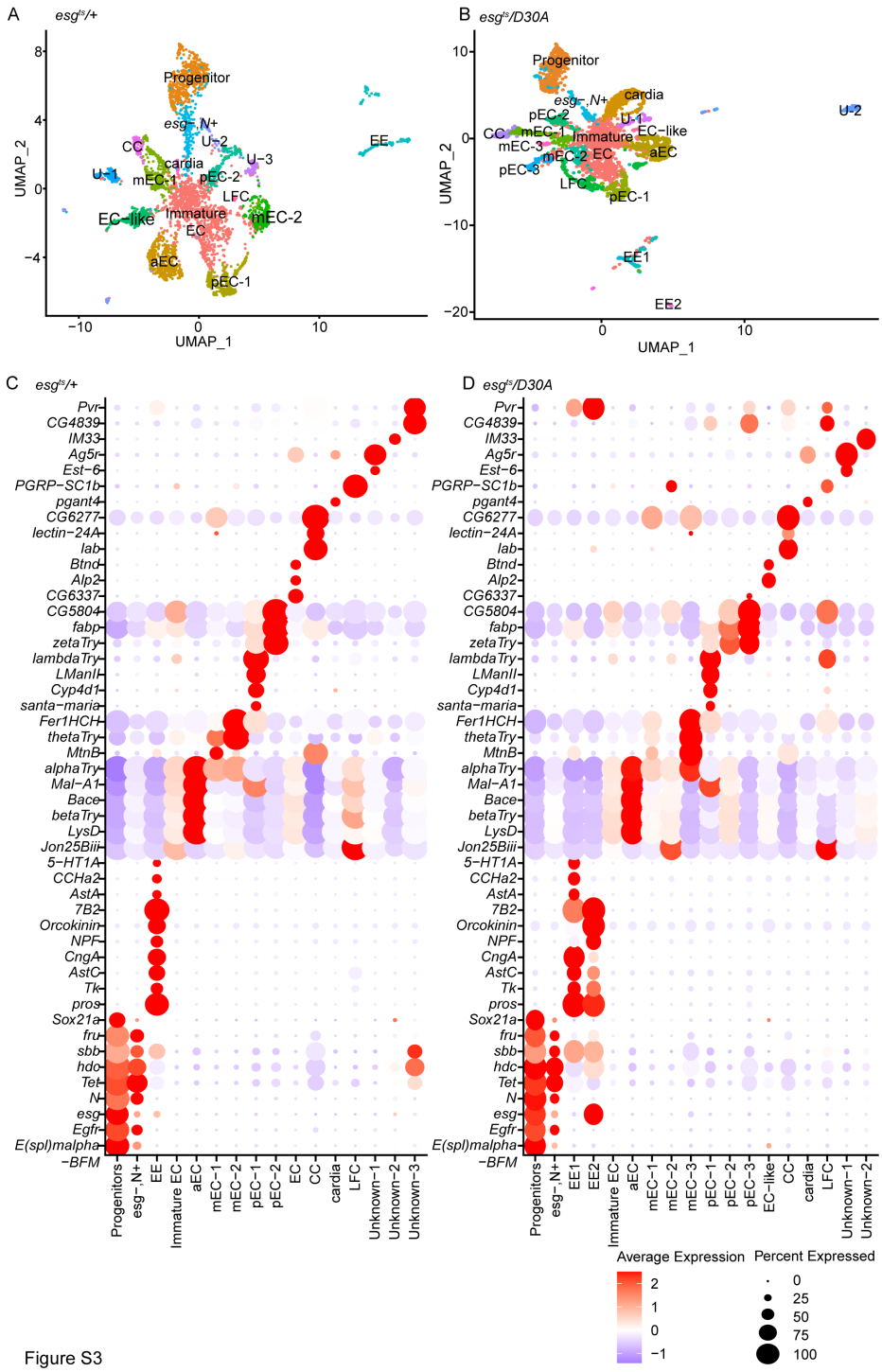

576 Figure S3

577 **Figure S3 A-B:** Two dimensional UMAP projection of cell types isolated from female control *esg^{ts}/+* intestines, and

578 from female *esg^{ts}/D30A* intestines, color coded by cell type. U = unknown, CC = copper cells, EC = enterocyte, EE

579 = enteroendocrine cell. **C-D:** Heatmap of IEC cluster markers colored by relative gene expression for flies of the

580 indicated genotypes. The size of the dot indicates the proportion of cells in each cluster that expressed the

581 indicated gene.

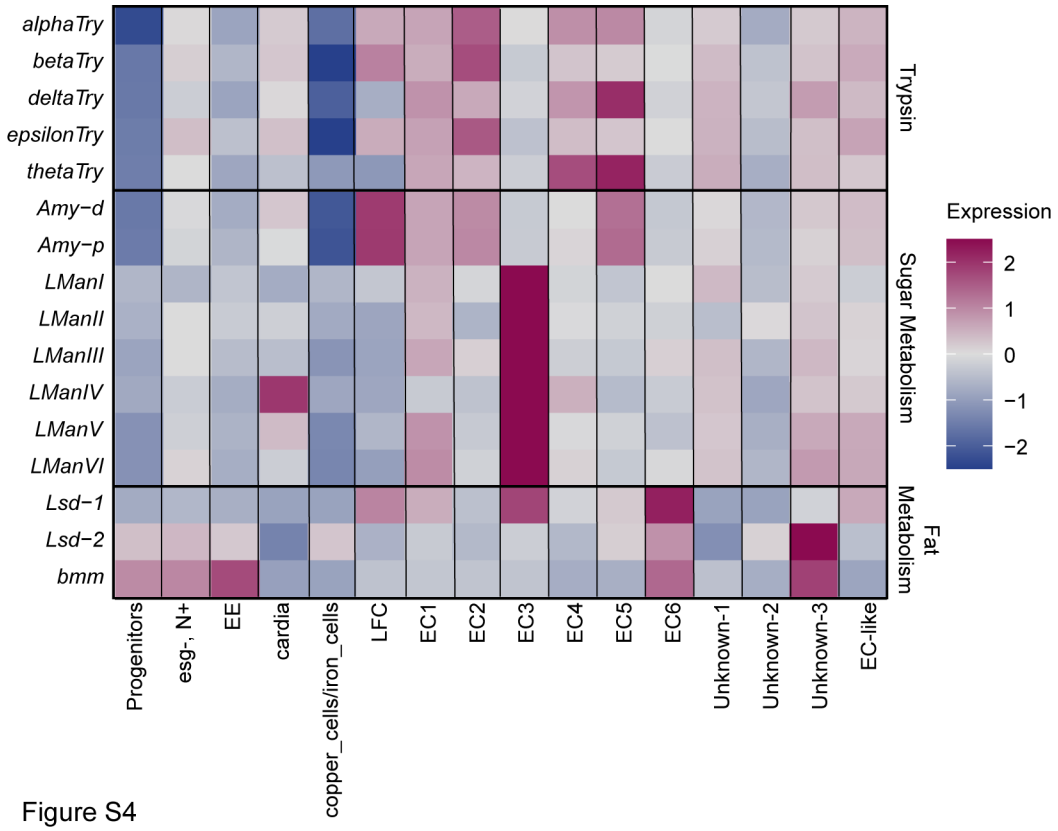

Figure S4

Figure S4: Heatmap showing relative cluster-average expression of metabolic enzymes (Try = *Trypsin*, Amy = *Amylase*, LMan = Lsysomal alpha-mannosidase, Lsd = Lipid storage droplet, bmm = *brummer*) in each intestinal epithelial cell type of control *esg*^{ts}*/+* flies.

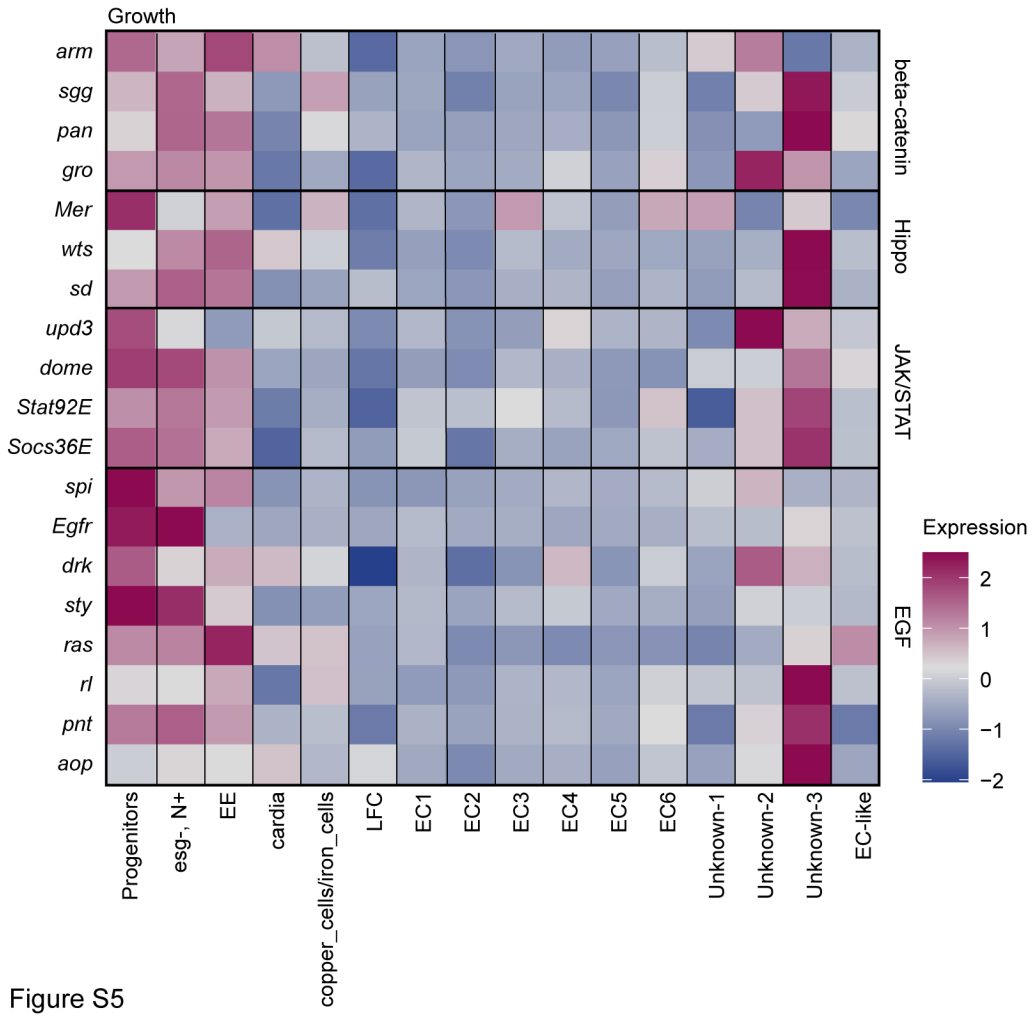

Figure S5

Figure S5: Heatmap showing relative cluster-average expression of prominent regulators of intestinal epithelial growth in each intestinal epithelial cell type of control *esg*^{ts}*/+* flies. For this analysis, we focused on indicated components of the beta-catenin, Hippo, JAK/STAT, and Epidermal Growth Factor (EGF) pathways.

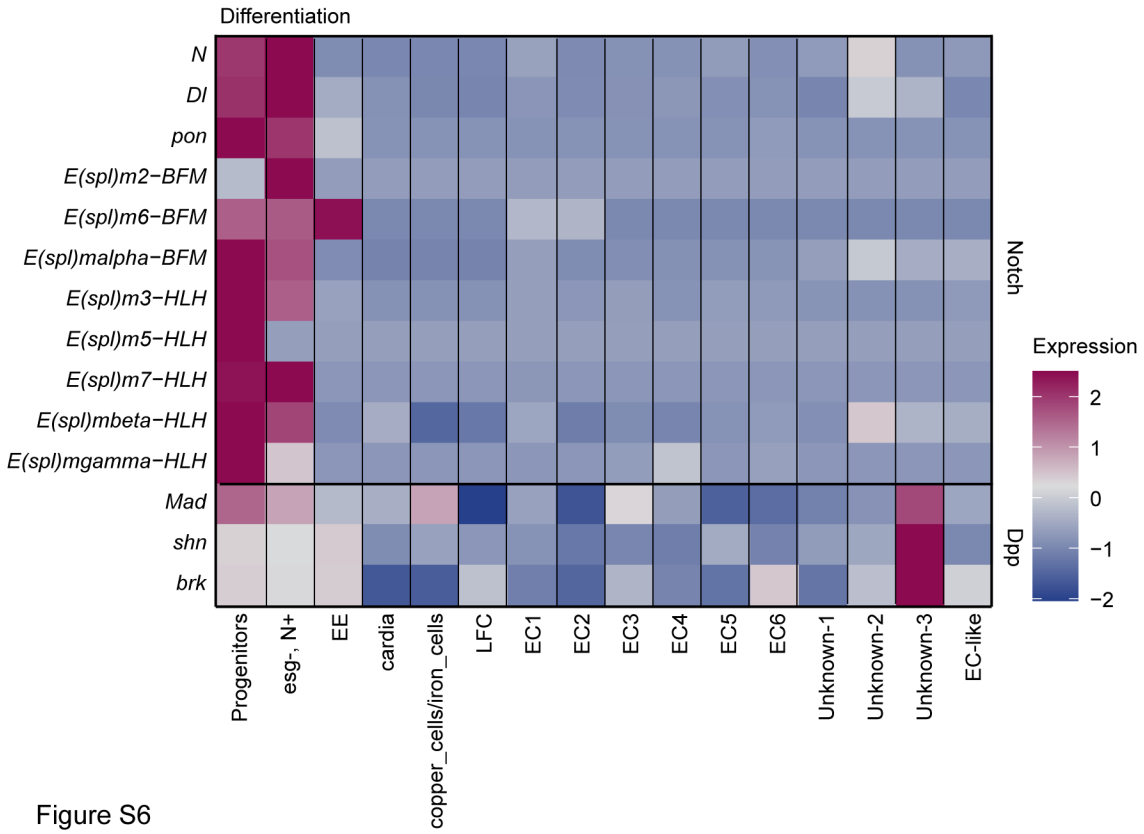

Figure S6

Figure S6: Heatmap showing relative cluster-average expression of prominent regulators of intestinal epithelial differentiation in each intestinal epithelial cell type of control *esg*^{ts}*/+* flies. For this analysis, we focused on indicated components of the Notch and Decapentaplegic (Dpp, *Drosophila* ortholog of Bone Morphogenetic Protein) pathways.

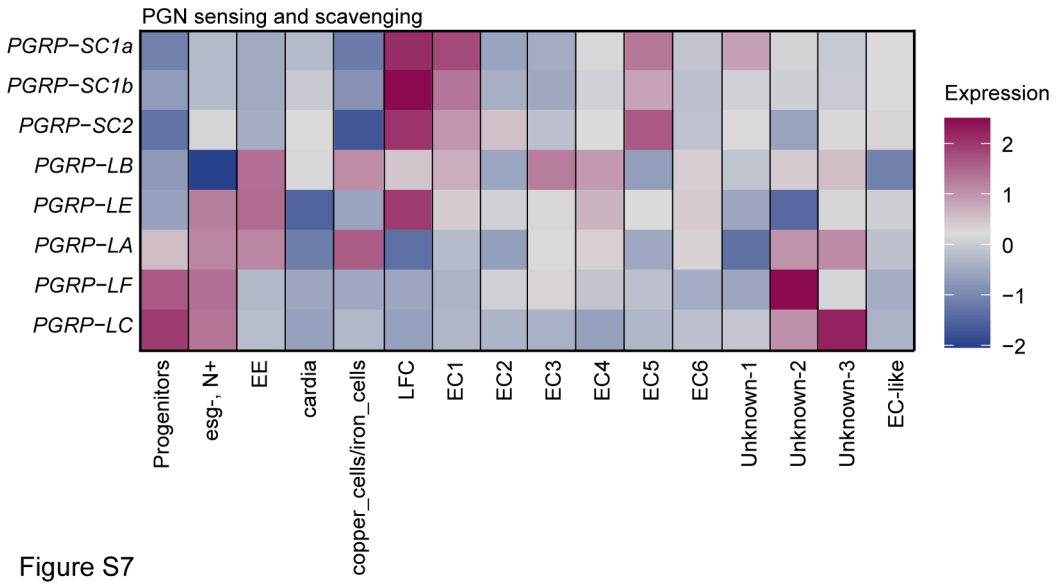

601 Figure S7

602 **Figure S7:** Heatmap showing relative cluster-average expression of prominent regulators of Peptidoglycan
603 detection (*PGRP-LE, LC, LA, LF*), and peptidoglycan amidases (*PGRP-SC1a, SC1b, SC2, LB*) in each intestinal
604 epithelial cell type of control *esg*^{ts}*/+* flies. For this analysis, we focused on Peptidoglycan Recognition Proteins
605 (PGRP) with detectable expression in the adult intestine.

606

607

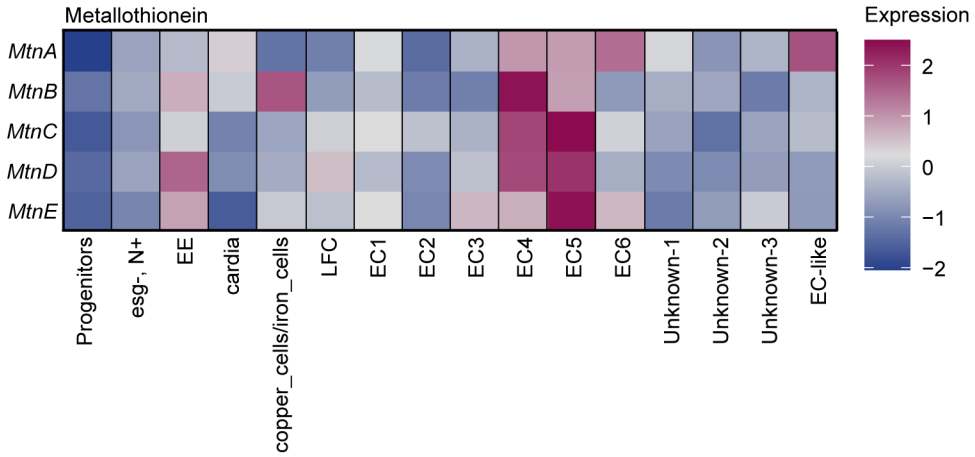

Figure S8

Figure S8: Heatmap showing relative cluster-average expression of prominent Metallothionein (*Mtn*) regulators of oxidative stress responses in each intestinal epithelial cell type of control *esg*^{ts}*/+* flies.

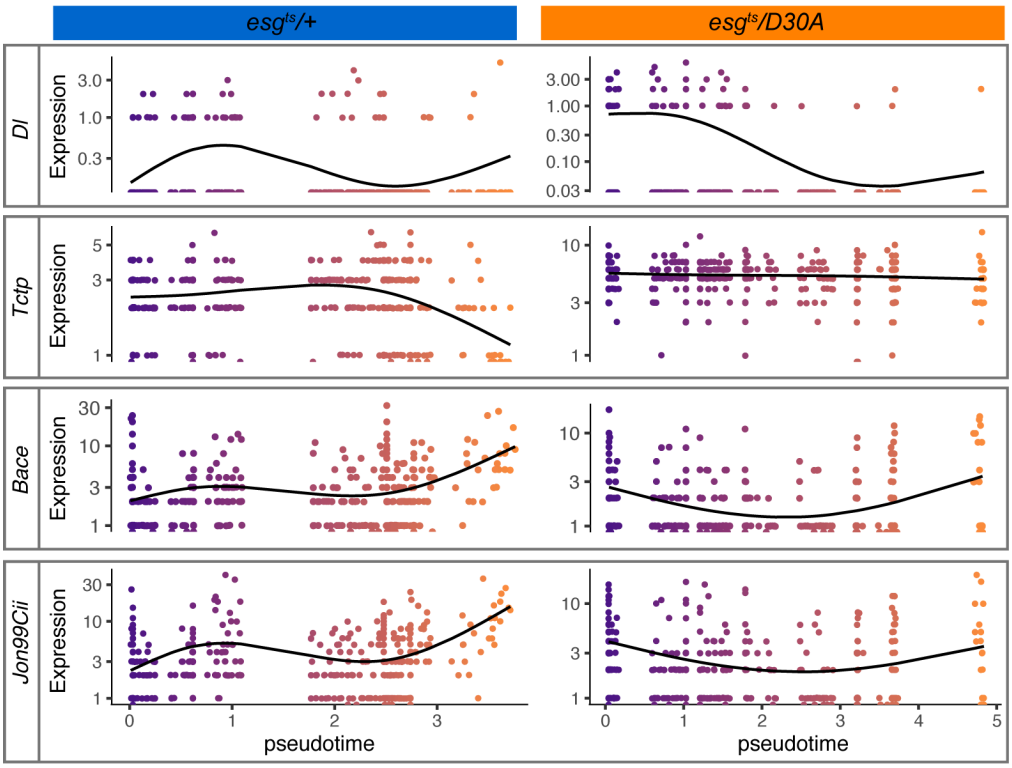

613 Figure S9

614 **Figure S9: Inhibition of IMD disrupts progenitor cell expression trajectories.** Expression of the stem cell marker

615 *Delta (Dl*), *Translationally-controlled tumor protein (Tctp),* and enterocyte markers *Bace* and *Jon99Cii* along

616 pseudotime in *esg^{ts}/+* and *esg^{ts}/D30A* progenitors. Dark purple marks cells at the beginning of pseudotime while

617 orange marks cells late in pseudotime. Black lines show expression trend.

618

619 **CITATIONS**

620 Bardin, A.J., Perdigoto, C.N., Southall, T.D., Brand, A.H., Schweisguth, F., 2010. Transcriptional
621 control of stem cell maintenance in the Drosophila intestine. Development 137, 705–714.
622 https://doi.org/10.1242/dev.039404
623 Barker, N., 2014. Adult intestinal stem cells: critical drivers of epithelial homeostasis and regeneration.
624 Nat. Rev. Mol. Cell Biol. 15, 19–33. https://doi.org/10.1038/nrm3721
625 Beehler-Evans, R., Micchelli, C.A., 2015. Generation of enteroendocrine cell diversity in midgut stem
626 cell lineages. Dev. Camb. Engl. 142, 654–664. https://doi.org/10.1242/dev.114959
627 Biteau, B., Jasper, H., 2014. Slit/Robo signaling regulates cell fate decisions in the intestinal stem cell
628 lineage of Drosophila. Cell Rep. 7, 1867–1875. https://doi.org/10.1016/j.celrep.2014.05.024
629 Biton, M., Haber, A.L., Rogel, N., Burgin, G., Beyaz, S., Schnell, A., Ashenberg, O., Su, C.-W., Smillie,
630 C., Shekhar, K., Chen, Z., Wu, C., Ordovas-Montanes, J., Alvarez, D., Herbst, R.H., Zhang, M.,
631 Tirosh, I., Dionne, D., Nguyen, L.T., Xifaras, M.E., Shalek, A.K., Andrian, U.H. von, Graham,
632 D.B., Rozenblatt-Rosen, O., Shi, H.N., Kuchroo, V., Yilmaz, O.H., Regev, A., Xavier, R.J.,
633 2018. T Helper Cell Cytokines Modulate Intestinal Stem Cell Renewal and Differentiation. Cell
634 175, 1307-1320.e22. https://doi.org/10.1016/j.cell.2018.10.008
635 Bosco-Drayon, V., Poidevin, M., Boneca, I.G., Narbonne-Reveau, K., Royet, J., Charroux, B., 2012.
636 Peptidoglycan Sensing by the Receptor PGRP-LE in the Drosophila Gut Induces Immune
637 Responses to Infectious Bacteria and Tolerance to Microbiota. Cell Host Microbe 12, 153–165.
638 https://doi.org/10.1016/j.chom.2012.06.002
639 Broderick, N.A., Buchon, N., Lemaitre, B., 2014. Microbiota-induced changes in drosophila
640 melanogaster host gene expression and gut morphology. mBio 5, e01117-01114.
641 https://doi.org/10.1128/mBio.01117-14
642 Brugman, S., 2016. The zebrafish as a model to study intestinal inflammation. Dev. Comp. Immunol.
643 64, 82–92. https://doi.org/10.1016/j.dci.2016.02.020
644 Buchon, N., Broderick, N.A., Chakrabarti, S., Lemaitre, B., 2009a. Invasive and indigenous microbiota
645 impact intestinal stem cell activity through multiple pathways in Drosophila. Genes Dev. 23,
646 2333–2344. https://doi.org/10.1101/gad.1827009
647 Buchon, N., Broderick, N.A., Lemaitre, B., 2013a. Gut homeostasis in a microbial world: insights from
648 Drosophila melanogaster. Nat. Rev. Microbiol. 11, 615–626.
649 https://doi.org/10.1038/nrmicro3074
650 Buchon, N., Broderick, N.A., Poidevin, M., Pradervand, S., Lemaitre, B., 2009b. Drosophila intestinal
651 response to bacterial infection: activation of host defense and stem cell proliferation. Cell Host
652 Microbe 5, 200–211. https://doi.org/10.1016/j.chom.2009.01.003
653 Buchon, N., Osman, D., David, F.P.A., Fang, H.Y., Boquete, J.-P., Deplancke, B., Lemaitre, B., 2013b.
654 Morphological and molecular characterization of adult midgut compartmentalization in
655 Drosophila. Cell Rep. 3, 1725–1738. https://doi.org/10.1016/j.celrep.2013.04.001
656 Capo, F., Chaduli, D., Viallat-Lieutaud, A., Charroux, B., Royet, J., 2017. Oligopeptide Transporters of
657 the SLC15 Family Are Dispensable for Peptidoglycan Sensing and Transport in Drosophila. J.
658 Innate Immun. 9, 483–492. https://doi.org/10.1159/000475771
659 Casali, A., Batlle, E., 2009. Intestinal stem cells in mammals and Drosophila. Cell Stem Cell 4, 124–
660 127. https://doi.org/10.1016/j.stem.2009.01.009
661 Couturier-Maillard, A., Secher, T., Rehman, A., Normand, S., Arcangelis, A.D., Haesler, R., Huot, L.,
662 Grandjean, T., Bressenot, A., Delanoye-Crespin, A., Gaillot, O., Schreiber, S., Lemoine, Y.,
663 Ryffel, B., Hot, D., Nùñez, G., Chen, G., Rosenstiel, P., Chamaillard, M., 2013. NOD2-mediated
664 dysbiosis predisposes mice to transmissible colitis and colorectal cancer. J. Clin. Invest. 123,
665 700–711. https://doi.org/10.1172/JCI62236

666 Dutta, D., Dobson, A.J., Houtz, P.L., Gläßer, C., Revah, J., Korzelius, J., Patel, P.H., Edgar, B.A.,
667 Buchon, N., 2015. Regional Cell-Specific Transcriptome Mapping Reveals Regulatory
668 Complexity in the Adult Drosophila Midgut. Cell Rep. 12, 346–358.
669 https://doi.org/10.1016/j.celrep.2015.06.009
670 Fast, D., Petkau, K., Ferguson, M., Shin, M., Galenza, A., Kostiuk, B., Pukatzki, S., Foley, E., 2020.
671 Vibrio cholerae-Symbiont Interactions Inhibit Intestinal Repair in Drosophila. Cell Rep. 30,
672 1088-1100.e5. https://doi.org/10.1016/j.celrep.2019.12.094
673 Ferguson, M., Foley, E., 2021. Microbial recognition regulates intestinal epithelial growth in
674 homeostasis and disease. FEBS J. https://doi.org/10.1111/febs.15910
675 Fu, Y.-Y., Egorova, A., Sobieski, C., Kuttiyara, J., Calafiore, M., Takashima, S., Clevers, H., Hanash,
676 A.M., 2019. T Cell Recruitment to the Intestinal Stem Cell Compartment Drives Immune-
677 Mediated Intestinal Damage after Allogeneic Transplantation. Immunity 51, 90-103.e3.
678 https://doi.org/10.1016/j.immuni.2019.06.003
679 Fukata, M., Chen, A., Klepper, A., Krishnareddy, S., Vamadevan, A.S., Thomas, L.S., Xu, R., Inoue, H.,
680 Arditi, M., Dannenberg, A.J., Abreu, M.T., 2006. Cox-2 is regulated by Toll-like receptor-4
681 (TLR4) signaling: Role in proliferation and apoptosis in the intestine. Gastroenterology 131,
682 862–877. https://doi.org/10.1053/j.gastro.2006.06.017
683 Fusunyan, R.D., Nanthakumar, N.N., Baldeon, M.E., Walker, W.A., 2001. Evidence for an Innate
684 Immune Response in the Immature Human Intestine: Toll-Like Receptors on Fetal Enterocytes.
685 Pediatr. Res. 49, 589–593. https://doi.org/10.1203/00006450-200104000-00023
686 Gendrin, M., Welchman, D.P., Poidevin, M., Hervé, M., Lemaitre, B., 2009. Long-Range Activation of
687 Systemic Immunity through Peptidoglycan Diffusion in Drosophila. PLOS Pathog. 5, e1000694.
688 https://doi.org/10.1371/journal.ppat.1000694
689 Guo, L., Karpac, J., Tran, S.L., Jasper, H., 2014. PGRP-SC2 promotes gut immune homeostasis to limit
690 commensal dysbiosis and extend lifespan. Cell 156, 109–122.
691 https://doi.org/10.1016/j.cell.2013.12.018
692 Guo, X., Yin, C., Yang, F., Zhang, Y., Huang, H., Wang, J., Deng, B., Cai, T., Rao, Y., Xi, R., 2019.
693 The Cellular Diversity and Transcription Factor Code of Drosophila Enteroendocrine Cells. Cell
694 Rep. 29, 4172-4185.e5. https://doi.org/10.1016/j.celrep.2019.11.048
695 Guo, Z., Ohlstein, B., 2015. Bidirectional Notch signaling regulates Drosophila intestinal stem cell
696 multipotency. Science 350. https://doi.org/10.1126/science.aab0988
697 Hsu, D., Fukata, M., Hernandez, Y.G., Sotolongo, J.P., Goo, T., Maki, J., Hayes, L.A., Ungaro, R.C.,
698 Chen, A., Breglio, K.J., Xu, R., Abreu, M.T., 2010. Toll-like receptor 4 differentially regulates
699 epidermal growth factor-related growth factors in response to intestinal mucosal injury. Lab.
700 Investig. J. Tech. Methods Pathol. 90, 1295–1305. https://doi.org/10.1038/labinvest.2010.100
701 Hugot, J.P., Chamaillard, M., Zouali, H., Lesage, S., Cézard, J.P., Belaiche, J., Almer, S., Tysk, C.,
702 O'Morain, C.A., Gassull, M., Binder, V., Finkel, Y., Cortot, A., Modigliani, R., Laurent-Puig, P.,
703 Gower-Rousseau, C., Macry, J., Colombel, J.F., Sahbatou, M., Thomas, G., 2001. Association of
704 NOD2 leucine-rich repeat variants with susceptibility to Crohn's disease. Nature 411, 599–603.
705 https://doi.org/10.1038/35079107
706 Hung, R.-J., Hu, Y., Kirchner, R., Liu, Y., Xu, C., Comjean, A., Tattikota, S.G., Li, F., Song, W., Sui,
707 S.H., Perrimon, N., 2020. A cell atlas of the adult Drosophila midgut. Proc. Natl. Acad. Sci. 117,
708 1514–1523. https://doi.org/10.1073/pnas.1916820117
709 Kamareddine, L., Robins, W.P., Berkey, C.D., Mekalanos, J.J., Watnick, P.I., 2018. The Drosophila
710 Immune Deficiency Pathway Modulates Enteroendocrine Function and Host Metabolism. Cell
711 Metab. 28, 449-462.e5. https://doi.org/10.1016/j.cmet.2018.05.026
712 Kim, C.-H., Paik, D., Rus, F., Silverman, N., 2014. The caspase-8 homolog Dredd cleaves Imd and
713 Relish but is not inhibited by p35. J. Biol. Chem. 289, 20092–20101.
714 https://doi.org/10.1074/jbc.M113.544841

715 Lee, J., Mo, J.-H., Katakura, K., Alkalay, I., Rucker, A.N., Liu, Y.-T., Lee, H.-K., Shen, C., Cojocaru,
716 G., Shenouda, S., Kagnoff, M., Eckmann, L., Ben-Neriah, Y., Raz, E., 2006. Maintenance of
717 colonic homeostasis by distinctive apical TLR9 signalling in intestinal epithelial cells. Nat. Cell
718 Biol. 8, 1327–1336. https://doi.org/10.1038/ncb1500
719 Leulier, F., Rodriguez, A., Khush, R.S., Abrams, J.M., Lemaitre, B., 2000. The Drosophila caspase
720 Dredd is required to resist gram-negative bacterial infection. EMBO Rep. 1, 353–358.
721 https://doi.org/10.1093/embo-reports/kvd073
722 Levy, A., Stedman, A., Deutsch, E., Donnadieu, F., Virgin, H.W., Sansonetti, P.J., Nigro, G., 2020.
723 Innate immune receptor NOD2 mediates LGR5+ intestinal stem cell protection against ROS
724 cytotoxicity via mitophagy stimulation. Proc. Natl. Acad. Sci. 117, 1994–2003.
725 https://doi.org/10.1073/pnas.1902788117
726 Lickwar, C.R., Camp, J.G., Weiser, M., Cocchiaro, J.L., Kingsley, D.M., Furey, T.S., Sheikh, S.Z.,
727 Rawls, J.F., 2017. Genomic dissection of conserved transcriptional regulation in intestinal
728 epithelial cells. PLoS Biol. 15, e2002054. https://doi.org/10.1371/journal.pbio.2002054
729 Micchelli, C.A., Perrimon, N., 2006. Evidence that stem cells reside in the adult Drosophila midgut
730 epithelium. Nature 439, 475–479. https://doi.org/10.1038/nature04371
731 Miguel-Aliaga, I., Jasper, H., Lemaitre, B., 2018. Anatomy and Physiology of the Digestive Tract of
732 Drosophila melanogaster. Genetics 210, 357–396. https://doi.org/10.1534/genetics.118.300224
733 Myllymäki, H., Valanne, S., Rämet, M., 2014. The Drosophila Imd Signaling Pathway. J. Immunol. 192,
734 3455–3462. https://doi.org/10.4049/jimmunol.1303309
735 Naito, T., Mulet, C., De Castro, C., Molinaro, A., Saffarian, A., Nigro, G., Bérard, M., Clerc, M.,
736 Pedersen, A.B., Sansonetti, P.J., Pédron, T., 2017. Lipopolysaccharide from Crypt-Specific Core
737 Microbiota Modulates the Colonic Epithelial Proliferation-to-Differentiation Balance. mBio 8.
738 https://doi.org/10.1128/mBio.01680-17
739 Neal, M.D., Sodhi, C.P., Jia, H., Dyer, M., Egan, C.E., Yazji, I., Good, M., Afrazi, A., Marino, R.,
740 Slagle, D., Ma, C., Branca, M.F., Prindle, T., Grant, Z., Ozolek, J., Hackam, D.J., 2012. Toll-like
741 Receptor 4 Is Expressed on Intestinal Stem Cells and Regulates Their Proliferation and
742 Apoptosis via the p53 Up-regulated Modulator of Apoptosis. J. Biol. Chem. 287, 37296–37308.
743 https://doi.org/10.1074/jbc.M112.375881
744 Neyen, C., Poidevin, M., Roussel, A., Lemaitre, B., 2012. Tissue- and ligand-specific sensing of gram-
745 negative infection in drosophila by PGRP-LC isoforms and PGRP-LE. J. Immunol. Baltim. Md
746 1950 189, 1886–1897. https://doi.org/10.4049/jimmunol.1201022
747 Nguyen, T.L.A., Vieira-Silva, S., Liston, A., Raes, J., 2015. How informative is the mouse for human
748 gut microbiota research? Dis. Model. Mech. 8, 1–16. https://doi.org/10.1242/dmm.017400
749 Nigro, G., Rossi, R., Commere, P.-H., Jay, P., Sansonetti, P.J., 2014. The cytosolic bacterial
750 peptidoglycan sensor Nod2 affords stem cell protection and links microbes to gut epithelial
751 regeneration. Cell Host Microbe 15, 792–798. https://doi.org/10.1016/j.chom.2014.05.003
752 Ogura, Y., Bonen, D.K., Inohara, N., Nicolae, D.L., Chen, F.F., Ramos, R., Britton, H., Moran, T.,
753 Karaliuskas, R., Duerr, R.H., Achkar, J.P., Brant, S.R., Bayless, T.M., Kirschner, B.S., Hanauer,
754 S.B., Nuñez, G., Cho, J.H., 2001. A frameshift mutation in NOD2 associated with susceptibility
755 to Crohn's disease. Nature 411, 603–606. https://doi.org/10.1038/35079114
756 Ohlstein, B., Spradling, A., 2007. Multipotent Drosophila intestinal stem cells specify daughter cell fates
757 by differential notch signaling. Science 315, 988–992. https://doi.org/10.1126/science.1136606
758 Ohlstein, B., Spradling, A., 2006. The adult Drosophila posterior midgut is maintained by pluripotent
759 stem cells. Nature 439, 470–474. https://doi.org/10.1038/nature04333
760 Paquette, N., Broemer, M., Aggarwal, K., Chen, L., Husson, M., Ertürk-Hasdemir, D., Reichhart, J.-M.,
761 Meier, P., Silverman, N., 2010. Caspase-mediated cleavage, IAP binding, and ubiquitination:
762 linking three mechanisms crucial for Drosophila NF-kappaB signaling. Mol. Cell 37, 172–182.
763 https://doi.org/10.1016/j.molcel.2009.12.036

764 Paredes, J.C., Welchman, D.P., Poidevin, M., Lemaitre, B., 2011. Negative Regulation by Amidase
765 PGRPs Shapes the Drosophila Antibacterial Response and Protects the Fly from Innocuous
766 Infection. Immunity 35, 770–779. https://doi.org/10.1016/j.immuni.2011.09.018
767 Petkau, K., Ferguson, M., Guntermann, S., Foley, E., 2017. Constitutive Immune Activity Promotes
768 Tumorigenesis in Drosophila Intestinal Progenitor Cells. Cell Rep. 20, 1784–1793.
769 https://doi.org/10.1016/j.celrep.2017.07.078
770 Price, A.E., Shamardani, K., Lugo, K.A., Deguine, J., Roberts, A.W., Lee, B.L., Barton, G.M., 2018. A
771 Map of Toll-like Receptor Expression in the Intestinal Epithelium Reveals Distinct Spatial, Cell
772 Type-Specific, and Temporal Patterns. Immunity 49, 560-575.e6.
773 https://doi.org/10.1016/j.immuni.2018.07.016
774 Ren, C., Webster, P., Finkel, S.E., Tower, J., 2007. Increased internal and external bacterial load during
775 Drosophila aging without life-span trade-off. Cell Metab. 6, 144–152.
776 https://doi.org/10.1016/j.cmet.2007.06.006
777 Ryu, J.-H., Kim, S.-H., Lee, H.-Y., Bai, J.Y., Nam, Y.-D., Bae, J.-W., Lee, D.G., Shin, S.C., Ha, E.-M.,
778 Lee, W.-J., 2008. Innate immune homeostasis by the homeobox gene caudal and commensal-gut
779 mutualism in Drosophila. Science 319, 777–782. https://doi.org/10.1126/science.1149357
780 Sancho, R., Cremona, C.A., Behrens, A., 2015. Stem cell and progenitor fate in the mammalian
781 intestine: Notch and lateral inhibition in homeostasis and disease. EMBO Rep. 16, 571–581.
782 https://doi.org/10.15252/embr.201540188
783 Spit, M., Koo, B.-K., Maurice, M.M., 2018. Tales from the crypt: intestinal niche signals in tissue
784 renewal, plasticity and cancer. Open Biol. 8, 180120. https://doi.org/10.1098/rsob.180120
785 Stöven, S., Ando, I., Kadalayil, L., Engström, Y., Hultmark, D., 2000. Activation of the Drosophila NF-
786 kappaB factor Relish by rapid endoproteolytic cleavage. EMBO Rep. 1, 347–352.
787 https://doi.org/10.1093/embo-reports/kvd072
788 Stoven, S., Silverman, N., Junell, A., Hedengren-Olcott, M., Erturk, D., Engstrom, Y., Maniatis, T.,
789 Hultmark, D., 2003. Caspase-mediated processing of the Drosophila NF-kappaB factor Relish.
790 Proc. Natl. Acad. Sci. U. S. A. 100, 5991–5996. https://doi.org/10.1073/pnas.1035902100
791 Takashima, S., Martin, M.L., Jansen, S.A., Fu, Y., Bos, J., Chandra, D., O'Connor, M.H., Mertelsmann,
792 A.M., Vinci, P., Kuttiyara, J., Devlin, S.M., Middendorp, S., Calafiore, M., Egorova, A., Kleppe,
793 M., Lo, Y., Shroyer, N.F., Cheng, E.H., Levine, R.L., Liu, C., Kolesnick, R., Lindemans, C.A.,
794 Hanash, A.M., 2019. T cell-derived interferon-γ programs stem cell death in immune-mediated
795 intestinal damage. Sci. Immunol. 4. https://doi.org/10.1126/sciimmunol.aay8556
796 Troha, K., Nagy, P., Pivovar, A., Lazzaro, B.P., Hartley, P.S., Buchon, N., 2019. Nephrocytes Remove
797 Microbiota-Derived Peptidoglycan from Systemic Circulation to Maintain Immune Homeostasis.
798 Immunity 51, 625-637.e3. https://doi.org/10.1016/j.immuni.2019.08.020
799 Vooijs, M., Liu, Z., Kopan, R., 2011. Notch: architect, landscaper, and guardian of the intestine.
800 Gastroenterology 141, 448–459. https://doi.org/10.1053/j.gastro.2011.06.003
801 Wallace, K.N., Akhter, S., Smith, E.M., Lorent, K., Pack, M., 2005. Intestinal growth and differentiation
802 in zebrafish. Mech. Dev. 122, 157–173. https://doi.org/10.1016/j.mod.2004.10.009
803 Wang, L., Sloan, M.A., Ligoxygakis, P., 2019. Intestinal NF-κB and STAT signalling is important for
804 uptake and clearance in a Drosophila-Herpetomonas interaction model. PLOS Genet. 15,
805 e1007931. https://doi.org/10.1371/journal.pgen.1007931
806 Wang, Z., Hang, S., Purdy, A.E., Watnick, P.I., 2013. Mutations in the IMD Pathway and Mustard
807 Counter Vibrio cholerae Suppression of Intestinal Stem Cell Division in Drosophila. mBio 4.
808 https://doi.org/10.1128/mBio.00337-13
809 Xu, N., Wang, S.Q., Tan, D., Gao, Y., Lin, G., Xi, R., 2011. EGFR, Wingless and JAK/STAT signaling
810 cooperatively maintain Drosophila intestinal stem cells. Dev. Biol. 354, 31–43.
811 https://doi.org/10.1016/j.ydbio.2011.03.018

812 Zaidman-Rémy, A., Hervé, M., Poidevin, M., Pili-Floury, S., Kim, M.-S., Blanot, D., Oh, B.-H., Ueda,
813 R., Mengin-Lecreulx, D., Lemaitre, B., 2006. The Drosophila amidase PGRP-LB modulates the
814 immune response to bacterial infection. Immunity 24, 463–473.
815 https://doi.org/10.1016/j.immuni.2006.02.012
816 Zeng, X., Hou, S.X., 2015. Enteroendocrine cells are generated from stem cells through a distinct
817 progenitor in the adult Drosophila posterior midgut. Development 142, 644–653.
818 https://doi.org/10.1242/dev.113357
819 Zhai, Z., Boquete, J.-P., Lemaitre, B., 2018. Cell-Specific Imd-NF-κB Responses Enable Simultaneous
820 Antibacterial Immunity and Intestinal Epithelial Cell Shedding upon Bacterial Infection.
821 Immunity 48, 897-910.e7. https://doi.org/10.1016/j.immuni.2018.04.010
822